NOVA SCHOOL OF SCIENCE & TECHNOLOGY

MATERIAL SCIENCES DEPARTMENT

TOMÁS ALEXANDRE DE SOUSA

Licenciado em Engenharia de Micro e Nanotecnologias

STRONG LIGHT-MATTER COUPLING FOR IMPROVED ORGANIC PHOTOVOLTAICS

MESTRADO EM ENGENHARIA DE MICRO E NANOTECNOLOGIAS

NOVA University of Lisbon
November, 2021

NOVA SCHOOL OF SCIENCE & TECHNOLOGY

MATERIAL SCIENCES DEPARTMENT

STRONG LIGHT-MATTER COUPLING FOR IMPROVED ORGANIC PHOTOVOLTAICS

TOMÁS ALEXANDRE DE SOUSA

Licenciado em Engenharia de Micro e Nanotecnologias

Orientador: Jaime Goméz Rivas, Full Professor,
Eindhoven University of Technology

Coorientadores: Manuel João de Moura Dias Mendes, Assistant Professor,
NOVA University Lisbon

Júri:

Presidente: Prof. Dr. Rodrigo Martins, Full Professor,
NOVA University Lisbon

Arguentes: Dr. Aleksandr Vaskin, Senior Investigator,
Eindhoven University of Technology

Vogais: Prof. Dr. Manuel João de Moura Dias Mendes, Assistant Professor,
NOVA University of Lisbon

MESTRADO EM ENGENHARIA DE MICRO E NANOTECNOLOGIAS

NOVA University of Lisbon
November, 2021

Strong Light-Matter Coupling for Improved Organic Photovoltaics

Para a minha família

ACKNOWLEDGEMENTS

The completion of this thesis represents a milestone in my life journey that resulted from work, effort and dedication over several years. Naturally, I feel great happiness and pride as I close this chapter and I would like to extend my thanks to all those who have accompanied me through this period.

First, I would like thank Professor Rodrigo Martins and Professor Elvira Fortunato, for creating the course I have enrolled in and for their inspiring dedication, leadership and commitment.

I would like to thank Professor Jaime Goméz Rivas, my advisor, for welcoming me and giving me the opportunity to work on this project. Thank you for the effort and all the attention you paid to me to carry out this project in view of the global pandemic situation.

I would also like to thank Professor Manuel Mendes, my co-advisor, for his support, calm and availability in the initial months when the course taken was still unclear.

Secondly, I would like to thank the institutions that hosted me, the NOVA School of Science and Technology of the University of Lisbon, as well as the Department of Materials Science, for motivating and encouraging their students to achieve their best. To Eindhoven University of Technology, for providing its students with an exceptional study and work environment.

Special thanks to my supervisor, Mohammed Saad, for all his patience with me, for the thousand and one explanations, for the mistakes made, for accompanying my work on weekends, for the constant support inside and outside the laboratory and for pushing me to excel in this project.

I would also like to thank the Surface Photonics and Semiconductors Nanophysics team, Ping, Matthijs, Stan and Ksenia whom always showed availability to help me when I needed it, and Tom van der Pol, from the Chemical Enginnering and Chemistry Department for his kindness and help on this project.

To my best friend, Myriam, who I have known since elementary school, I want to thank you for all the moments spent, all the conversations, all the advice, all the joyful laughs, all the good and bad moments that are part of our friendship and above all for being present even from a distance.

A special thanks to Amanda for her moments of support, motivation, moments of panic and despair, moments of craziness and adventures and for the dreams that came true thanks to our joint effort and dedication over the last few years. Thank you Leonor, for all the inumerous and great moments that fit within your mini cooper and for the endless nights of support and laughs.Thanks to all my college colleagues, Inês, Bernardo, Viana, Joana, Rita, and Gil who accompanied me throughout these years, for all the moments of study, breaks, laughs, socializing and group work.

There are no words to express how much I thank my family, my parents, Antonino and Telma, my grandparents, Natividade, Faustino, Lopes and Chico, my brother Tiago, Sandra, Ina, Tó, Paula and Rafaela for all the love, affection, friendship, support, advice, teachings, fun and strength that they transmitted to me and without which I would not have been able to get where I am, a huge thank you.

“Not all those who wander are lost.”

-J.R.R. Tolkien

ABSTRACT

Organic photovoltaic technology is a very promising area of research - potentially able to balance the current energy demand the world requires every day. Organic materials inherit fascinating properties like tailorable optical properties, adjustable optical bandgap and electrical conductivity, and easy and cheap processing among others. These materials also present short exciton diffusion lengths, low charge mobilities and weak absorption, negatively impacting the short-circuit current (Jsc) and open-circuit voltage (Voc) of organic solar cells and their performance. Light-matter coupling is an exponentially growing field of research, which focuses on the coupling of photonic modes and excitonic states of matter. This interaction results in the formation of hybrid states of matter - polaritons - with interesting new properties. The pioneer work of incorporating this concept in optoelectronic devices has allowed for improved photoconductivity, long-range energy transfer, reduced optical losses, higher harvesting rates and enhanced power conversion efficiencies. The work of this thesis focuses on the simulation, fabrication, and characterization of organic solar cells with a nanostructured layer to optimize its short-circuit current, as well as simpler systems of metallic lattices to study strong coupling between collective plasmonic resonances and organic excitons in standard donor-acceptor blends. Full solar cells devices containing square gold lattices were achieved. The open-circuit voltage and fill factor (FF) retrieved through J-V curves remained roughly unchanged whereas the short-circuit is slightly reduced. Although the investigated solar cells do not show evidence of strong coupling as they were not optimized, these measurements illustrate that it is possible to structure the electrode of the cell with a structure supporting optical modes without degrading the Voc. External quantum efficiency analysis provided an insight on how the gold lattices influence the quantum efficiency spectrum of the the solar cells, allowing the absorption edge to be shifted towards lower energies in some cases.

Keywords: Organic photovoltaics, Strong light-matter coupling, Surface lattice resonances

RESUMO

A tecnologia de fotovoltaicos orgânicos é um campo de pesquisa bastante promissor - potencialmente capaz de equilibrar a atual procura energética a nível mundial. Os materiais orgânicos possuem propriedades fascinantes tais como a adaptabilidade de propriedades óticas, ajustabilidade do hiato ótico e condutividade elétrica, apresentando um custo reduzido e facilidade de fabrico, entre outros. Por outro lado, estes materiais também possuem cumprimentos de difusão de excitões bastante curtos, mobilidades de carga baixas e baixa absorção, o que influencia negativamente a corrente de curto-circuito (Jsc) e a tensão de circuito aberto (Voc) de uma célula solar orgânica e, consequentemente, o seu desempenho. A área da física que estuda o *coupling* entre luz e matéria encontra-se num crescimento exponencial, focando-se principalmente no acoplamento de modos fotónicos e excitões. Esta interação resulta na formação de estados híbridos de matéria - polaritões - que possuem novas propriedades interessantes. O trabalho pioneiro de incorporar este conceito em dispositivos optoeletrónicos com matrizes nano estruturadas permitiu uma melhoria da fotocondutividade, uma transferência de energia a longo alcance, redução de perdas ópticas, recolhas de cargas mais altas e eficiências de conversão de energia superiores nestes dispositivos. Este trabalho foca-se em simular, fabricar e caracterizar células solares orgânicas com um electrodo nano estruturado, bem como sistemas mais simples de matrizes metálicas cujo objetivo é estudar o *strong coupling* entre ressonâncias coletivas e excitões orgânicos que resultam de misturas orgânicas de camadas doadoras e aceitadoras *standard* na industria. Neste trabalho foram realizados dispositivos de células solares contendo matrizes de ouro de forma a maximizar a Jsc destas, bem como sistemas mais simples de matrizes metálicas para estudar *strong coupling* entre estas e modos excitónicos. A tensão de circuito aberto e o fator de forma (FF), extraídos através das curvas J-V, permaneceram praticamente inalterados, enquanto que a corrente de curto-circuito sofreu uma ligeira redução. Apesar das células solares investigadas não apresentarem quaisquer evidência de *strong coupling* dado que estas não se encontram totalmente otimizadas, estas medições provam que é possível modificar um elétrodo, de forma a que este suporte modos óticos, sem que haja uma degradação da tensão de circuito aberto.A análise da eficiência quântica externa forneceu uma visão sobre como as matrizes de ouro influenciam fortemente a forma da eficiência quântica, permitindo que a fronteira de absorção se desloca-se para energias mais baixas em alguns casos.

Palavras-chave: Fotovoltaicos orgânicos, *Strong light-matter coupling*, *Surface lattice resonances*

CONTENTS

LIST OF FIGURES

LIST OF TABLES

SYMBOLS

V_{OC}	Open circuit voltage
J_{SC}	Short circuit current
FF	Fill factor
IPA	Isopropanol
PMMA	Polymethyl methacrylate
MIBK	Methyl isobutyl ketone

ACRONYMS

AFM	Atomic force microscopy
EBL	Electron beam lithography
EM	Electromagnetic
ETL	Electron transport layer
FDTD	Finite-difference time-domain
HTL	Hole transport layer
IP	In-plane
ITO	Indium-tin-oxide
LSP	Localized surface plasmon
LSPR	Localized surface plasmon resonance
NIR	Near infrared
NP	Nanoparticle
OOP	Out-of-plane
OPV	Organic photovoltaic
OSC	Organic semiconductor
PCE	Power conversion efficiency
PS	Polysterine
PV	Photovoltaic
RA	Rayleigh anomalies
RPM	Rotations per minute
SEM	Scanning electron microscopy
SLR	Surface lattice resonance
TE	Transverse electric
TM	Transverse magnetic
UPW	Ultra pure water
UV	Ultraviolet

1.
MOTIVATION AND OBJECTIVES

The growth of the human population leads to an increased pressure on the world's energy resources, putting at risk the planet's sustainability. Solar energy is a renewable source, widely available, and that can potentially fill the gap between the constant demand and supply for energy consumption through photovoltaic (PV) devices - converting sunlight energy into electricity [1][2]. Among all types of PV technologies, the one based in organic materials, i.e. organic photovoltaics (OPV) is unquestionably attractive due to the vast advantages inherited from organic material properties - tunable optical properties, mechanical flexibility, adjustable optical band-gap and electrical conductivity, low environmental impact and low cost [1], [3]–[8].

However, organic materials also share a few undesirable properties which strongly impact the performance of OPV. Short exciton diffusion lengths, weak absorption and low charge mobilities are among the main organic material properties which negatively affects the short-circuit current (Isc) and the open-circuit voltage (Voc), lowering the power conversion efficiency (PCE) of an OPV cell [6], [7], [9][10].

Light-matter coupling is a rapidly growing field of research, which describes the coupling between photonic modes and excitons in matter. Strong coupling in solid-state cavities leads to the emergence of new hybrid states of matter, known as polaritons, when the energy exchange rate between the photonic mode and the excitons surpasses the loss rates of the system [11]–[13]. These polaritons possess interesting new properties inherited from light. Thus, the incorporation of this new concept on optoelectronic devices - so called polaritonic devices - has resulted in improved photoconductivity, long-range energy propagation, reduced optical losses, higher energy transfer rates, higher exciton harvest rates and higher power conversion efficiencies [9], [11], [14].

Therefore, solid-state cavities with interesting geometries - such as the open distributed feedback cavity - supporting strong light-matter coupling have been studied. In this cavity, the active layer is close to a nanostructured grating electrode, capable of supporting collective plasmonic resonances, such as the ones stemming from nanodisk arrays [15]–[17].

The coupling of the localized surface resonances of the individual particles, enhanced by in-plane light diffraction (Rayleigh anomalies), results in surface lattice resonances (SLRs) with low radiative losses, narrow line widths and high-quality factors. SLRs enable high field enhancements over large volumes combined with longer lifetimes. In addition, these structures present a tailorable nature - the surface lattice resonance energy can be tuned by adjusting the diameter, height and spacing of the nanoparticles in the lattice [12], [15], [18], [19]. These novel structures are undeniably interesting to incorporate in organic photovoltaic devices, aiming to improve them. The goal of this work is to simulate, fabricate and characterize organic solar cells with a nanostructured electrode to maximize its short-circuit current as well as simpler systems of metallic lattices to study strong light-matter coupling between collective resonances and organic excitons in standard donor-

acceptor systems. For that end, numerical simulations to define the most promising geometry for nanodisk arrays and organic solar cells are performed. Electron-beam lithography will be used to fabricate nanoparticle array samples and to define the final array structures onto the organic solar cells - followed by the respective optical, morphological, and electrical characterization of the devices.

2. INTRODUCTION

2.1. Organic photovoltaic technology

The human population has experienced exponential growth in the past century. Nowadays, different types of energies are explored to sustain the energetic needs of approximately eight billion people. Among all sources of energy, solar energy holds great potential to fill the large gap between the daily energy demand and supply. Sunlight is a renewable source of energy that is widely available around the planet, allowing it to be harvested by photovoltaic (PV) devices that can convert light into electricity. [1][2]

The photovoltaic devices can be roughly divided into two types: inorganic photovoltaics and organic photovoltaics (OPV) [1]. Inorganic PV is a relatively mature technology with considerable performance. However, this silicon-based technology is very energy-intensive as a result of its fabrication procedure. The industry market requires a new non-energy-intensive material, which can match the silicon-technology efficiency [3][4]. Organic materials are unquestionably attractive because they ensure tunable optical properties, mechanical flexibility, potential low-cost materials, low environmental impact, adjustable band-gap, and electrical conductivity. [1], [3]–[8]

The core of an organic photovoltaic device is the organic materials donor and acceptor layers. These layers are composed of π-bonded organic materials such as polymers, dendrimers, oligomers, etc., normally composed of carbon and hydrogen atoms. [5], [20]

The working mechanism of the organic solar cells is as follows: when an incident photon excites an electron of the organic donor layer, an electron-hole pair is created, known as an exciton. The exciton charges are bound by Coulomb attractions and must be dissociated to generate current in the device. This exciton must reach the interface between the donor and acceptor materials to be dissociated before it recombines to its original energy state [1], [3], [4]. A bulk heterojunction structure is commonly used in OPV devices. In this cell structure, the donor and acceptor materials are mixed, forming an organic blend so, the superficial area of the donor and acceptor material is increased, compared to traditional biplanar structures. In this case, more excitons will be able to reach the interface between the acceptor and donor materials, which is relatively large compared with the bilayer structure, and dissociate.[2].

The power conversion efficiency of a solar cell is linearly dependent on the short-circuit current (Isc), filling factor (FF), and open-circuit voltage (Voc), which can be attained through Equation (1) and (2), respectively [10][21],

$$I(V) = I_{SC} - I_0 \left[exp\left(\frac{qV - IR_S}{\gamma kT}\right) - 1 \right] - \frac{(V - IR_S)}{R_{SH}}, \quad (1)$$

$$V_{OC} = \frac{\gamma kT}{q} \ln\left(\frac{I_{SC}}{I_0} + 1\right). \quad (2)$$

Where q is the elemental charge, T is temperature, k is Boltzmann's constant, γ is the diode-quality factor, R_s is the series resistance and R_{sh} is the shunt resistance.

To compare photovoltaic devices with different active areas, the current must be normalized to the area-current density (J). Some of the most important parameters are pinpointed in the J-V curve figure below - Figure 2.1.

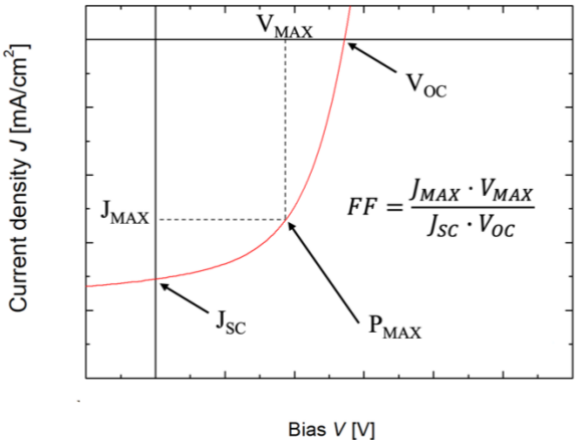

Figure 2.1 - Representation of a J-V curve (in red), with the respective maximum voltage (Vmax), maximum current density (Jmax), open-circuit voltage (Voc), short-circuit current density (Jsc) and maximum power (Pmax) parameters identified and fill factor (FF).

Short-circuit current (Jsc) is defined as the measured current at zero bias voltage, while the open-circuit voltage (Voc) is the voltage measured when the current is zero. The maximum power is achieved for the highest value of the product between J and V. At this point, J and V are defined as J_{max} and V_{max}. Another important parameter for these devices is the fill factor, calculated by the ratio between $J_{max} \cdot V_{max}$ and $J_{sc} \cdot V_{oc}$, as seen in Figure 2.1. Lastly, the device's efficiency is written as

$$\eta = \frac{J_{SC} V_{OC} FF}{P_{IN}} \quad (3)$$

Where η is the efficiency and P_{IN} is the incident light power on the cell, which in AM1.5 standard condition test spectrum is 100 mW/cm^2.

Another important photovoltaic characterization is the external quantum efficiency (EQE) which is defined as the ratio between the number of collected charges by the solar cell and the number of incident photons for a specific energy [22].

For organic materials, the average exciton diffusion length is approximately 10-20 nm. These short diffusion lengths, combined with low charge mobilities and weak absorptions, negatively affect the J_{sc} and V_{oc} of an organic solar cell, limiting the photo-electrical efficiency of this technology [9].

Over the years, the scientific community has focused on improving OPV technology, attaining over 16% PCE in these devices, however, the diffusion lengths, charge mobilities, and absorption rates in organic photovoltaics stands as the ultimate bottleneck [6], [7].

Strong light-matter coupling in organic materials is an exponentially growing research field that has allowed the emergence of interesting material properties such as long-range energy transfer [23][24], enhanced exciton transport, polariton lasing, among others, due to the presence of hybrid light-matter states called exciton-polaritons. These states are compelling to exploit in optoelectronic devices operating under strong coupling - polaritonic devices - and more specifically in organic photovoltaics [17], [25], [26].

2.2. **Strong light-matter coupling**

Polaritons are quasiparticles that arise from a strong coupled light and matter interaction [11], [27]–[29]. The strong coupling regime is achieved when the exchange of energy between the photonic mode and the excitons surpasses the loss rates of the system, leading to exciton-polaritons states [11]–[13]. The energy exchange (in a strong coupling system) through time will result in a splitting of the resonant energy in frequency - Rabi splitting - and lower polariton and upper polariton bands are established, Figure 2.2. The splitting can be observed in a dispersion diagram as an avoided crossing (anticrossing), where the uncoupled system modes intersect [30].

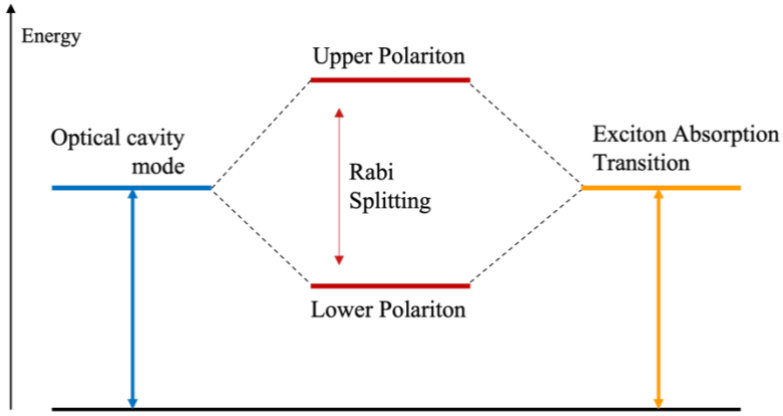

Figure 2.2 - Strong light-matter coupling diagram of two uncoupled states, represented in blue and yellow, of an optical cavity mode and an exciton mode, respectively. The exchange of energy between these two modes through time will lead to a splitting of the resonant energy splitting in frequency, Rabi Splitting, establishing the upper and lower polariton bands.

Light can propagate fast due to its low effective mass, this characteristic can be exploited through strong coupling, where the excitons can benefit from this property. In other words, it is possible to enhance material properties through strong coupling, allowing long-range and faster charge transfer [31].

Organic materials are an excellent candidate for polaritonic devices since they present a large dipole transition moment, sufficiently narrow linewidths, and they can support strong light-matter coupling at room temperature [31]. Thus, OPVs can benefit from strong light-matter coupling to reduce the limitations of these devices: low power conversion efficiency resulting from the short exciton diffusion lengths and charge recombination losses, photodegradation, and poor charge transfer along with the donor and acceptor layers' interface [16].

The formation of the new polariton peaks allows to extend the boundaries of the OPVs. These states allow to enhance the absorption range of the organic devices and tune its optical gap while unaffecting the open-circuit voltage (Voc) - as reported by Nikolis et al. [9] - inducing a reduction in optical losses (given by Eopt - qVoc). For some devices, strong coupling allowed to steepen the absorption edge. Combining the latter with low electron transfer driving force, Nikolis et al. demonstrated that the energy losses in this organic device is comparable with other PV technologies records.

Light-matter coupling has demonstrated exciton transport enhancements due to the delocalized nature of the polariton, inherited from light. In Ref.[11], Wang et al.have reported an effective increase of exciton harvest rate by one magnitude order, by strongly coupling an organic planar heterojunction to an optical cavity mode. Wang et al. based their system on nature's photosynthesis to efficiently channel charge states to the donor/acceptor interface, improving energy transfer by two- to threefold. Despite the separated charge extraction is not optimized in their system, Wang et al. state that this concept can be applied in organic systems under strong coupling to improve the photon-to-current efficiency.

Real-time long-range transport in organic materials under strong coupling is made possible by ultrafast time-resolved microscopy, as observed by Rozenman G. et al. in Ref. [14]. The results show the propagation velocity of polaritons is 0.2-0.4 microns/psec. Their studies not only show the path to explore polariton dynamics in strongly coupled organic systems, but also demonstrate that strong coupling enhanced the exciton transport, typically in the nanometer scope, to the micrometer scale.

Engineering solid-state cavities and tuning them to achieve strong light-matter coupling is one way of improving solar cell devices. Nevertheless, by studying different organic blend and their ratio can also improve photovoltaic performance as the study by Yao et al. suggests, where the crucial impact of donor/acceptor ratio in PM6:Y6 organic blend system was investigated - an exciting 10% PCE was achieved for blends with 10% donor ratio, derived from efficient charge separation, transport, and slow recombination [32].

Most of the earlier work regarding strong coupling has been based on Fabry Perot solid-state cavities. In these cavities, an active layer is confined in-between two mirrors [9], [33]. The closed geometry of these cavities limits their application for organic photovoltaics, where the active layer must absorb the highest percentage of incident light.

Distributed feedback cavities have gained attention in recent years as a promising structure for organic photovoltaic technology. In these structures, the active layer is located near a nanostructured grating layer, capable of confining light. These open cavities are quite interesting to be incorporated in OPV technology considering they are capable of supporting strong light-matter coupling. In addition, they also allow a better in- and out-coupling of light and an improved coupling stemming from the mode volume of the grating structures.

2.3. **Surface Lattice Resonances**

Optical resonances in nanostructures have opened new paths to manipulate the light. These resonances allow for local field enhancements and increase light-matter interaction, which can be exploited in light harvesting devices.

When light shines upon metal nanoparticles, these exhibit coherent oscillations of their free electrons, i.e., localized surface plasmon (LSP) resonances, which allow local field enhancements in nanometric volumes. However, a enhancement over larger volumens is required for many applications such as surface enhanced spectroscopies, solid-state lighting, lasing, or sensing [15][34]–[37].

Collective resonances of individual nanoparticles in a periodic lattice have received attention in recent years due to their low radiative losses, narrow line widths and higher quality factors [15]. The radiative coupling of the localized resonance induces collective lattice resonances. The latter can be further enhanced by in-plane light diffraction orders - Rayleigh anomalies (RAs) - resulting surface lattice resonances (SLRs) [38].

SLRs combine both plasmonic and photonic properties - high field enhancements over large volumes mostly due to RAs (arising from plasmonic nanostructures) combined with longer lifetimes (which result from the photonic array structure), having exciting applications perspectives such as in sensing, optical filtering, and fluorescence enhancement [19]. In addition, SLRs present a tailorable nature over the wide band of wavelengths [39], [40] - by adjusting the diameter, height and spacing of the individual particles, [19][18][41].

For arrays of metallic nanoparticles, SLRs have a dispersive behavior since the surrounding refractive index and the periodicity of the array ultimately determines the diffraction of the scattered waves [42]. Thus, a dispersion diagram, i.e. energy as a function of wave vector, can be plotted if the sample is illuminated with a collimated white light beam with a transverse magnetic (TM) or transverse electric (TE) polarization.[12]

As already mentioned, most of the work on strong light-matter coupling is based on Fabry-Perot microcavities. However, these cavities are not useful for organic photovoltaics applications as the short circuit current is low by the limited light absorption. On the other hand, Bai P. et al. investigated the coupling between semiconductor polymer (P3HT) excitons and the optical modes in an open aluminum square-array resonant cavity. Through finite-difference time-domain simulations combined with a particle swarm optimization algorithm, they determined the optimal lattice parameters to achieve strong light-matter coupling, presenting a maximum Rabi splitting of 0.8 eV and illustrating an effective approach for optimizing open cavities based on lattice structures with applications in OPVs [16].

Extensive interest has been placed in investigating metallic collective lattice resonances, whereas dielectric systems remain quite unexplored. Castellanos G. et al. has conducted a numerical investigation on lattice resonances where part of their work focuses on a silicon hexagonal lattice system embebbed within a symmetric dielectric medium, maximizing the radiative in-plane coupling between the nanoparticles. Their work provides an in-depth description on the field distribution and intensity enhancement, which are most valuable for applications, such as photovoltaics [15].

Hüttenhofer et al. have demonstrated the possibility of enhancing the photon-to-electron conversion efficiency on semiconductors by introducing nanoimprinted amorphous gallium phosphide nanodisks in a square lattices on indium tin oxide (ITO). Nanoimprinted nanodisks lead to enhance the photocurrent by more than five times comparing to a planar film. This was achieved by combining lattice resonances with anapole excitations, which consist of excitations that suppress backscattering and that are capable of confining light, thus leading to high EM field strengths within the material. The method employed is not material dependent, allowing also for industrial scalability and high throughput of nanopatterned surfaces production [43].

Long-range energy transfer is crucial in organic polaritonic devices, where diffusion lengths are short by the organic material nature. Yadav et al. studies provide insight on long-range energy transfer in a nanostructured layer. A silver nano disk lattice was introduced in a semiconductor medium composed of quantum dots. Photoluminescence measurements not only proved the existence of polariton states but also allowed to measure the extention of their propagation. Their work demonstrated an exciting experimental energy propagation of 600 μm and an insight on how this length is affected by the coupling strength of the system [44].

One interesting way of controlling the coupling strength in plasmonic cavities has been shown by Berghuis A. et al. In their work, a silver nanoparticle array SLR is coupled to tetracene single crystals excitons. By solely changing the crystal orientation (and therefore, the exciton transition dipole moment), with respect to the cavity field, enabled to change the Rabi splitting energy from 39 to 142 meV. They also observed a shift in the lower polariton energy depending on the crystal orientation - achieving 2.28 eV and 2.33 eV for parallel and perpendicular orientations, respectively[17].

3. METHODS AND MATERIALS

3.1. Finite-difference time-domain simulations

Finite-difference time-domain (FDTD) simulations were implemented to optimize the light-matter coupling strength between metallic lattices resonances and the excitons in PDPPT5T:IEICO-4F organic blend.

Two different structures were designed to study the SLRs induced by the Au NP arrays and the polariton bands that arise from the coupling of organic excitons with the SLRs.

A nanoparticle, composed of a 50 nm gold layer on top of a 2 nm Ti layer, was placed above a glass layer with a refractive index of 1.47. To determine the resonances of the particle, it was embebbed in a 150 nm thick medium with n=1.96 and air on top. In other simulations, the particle was surrounded by a 150 nm thick layer of PDPPT5T:IEICO-4F organic blend to simulated the response of a single nanoparticle.

A 3D refined mesh of 2 x 2 x 1 nm, in X, Y and Z respectively, was also added to the region of interest for the FDTD simulation. The power absorbed and the extinction for these structures were calculated.

Additional numerical simulations were implemented to optimize the short-circuit current in full solar cell devices containing metallic lattices, by varying the lattice diameter and period, and the organic blend thickness.

A particle swarm optimization (PSO) methodology was adopted to optimize the organic blend height and the lattice diameter and pitch, to achieve the maximum J_{sc} in the full device simulations. Thus, the fitness parameter for the PSO was the short-circuit current of the device. PSO algorithms are designed to optimize numerical problems by searching the best solution in a defined random population of candidate solutions - "particles". These can move or evolve through the seach space by changing their velocity and/or position. The movement of each candidate "particle" is determined by its local best position and the best known position of different "particles". Ultimately, the following generations will converge to the global best solution. [45]

The PSO was set for 30 populations through 50 generations, where the organic blend thickness was restricted to the range from 30 to 100 nm, the lattice diameter to the range from 60 to 200 nm and the particles pitch to the range from 300 to 600 nm.

3.2. Gold nano disks arrays fabrication

Firstly, two beakers containing acetone and isopropyl alcohol (IPA) were prepared to place the samples in ultrasonic baths for 15 minutes each, in that same order. Lastly, the samples were dried with N_2 gas.

Afterwards, an A4 950K PMMA volume of roughly 470 µL was spin-coated on the glass sample at 3500 RPM for 1 minute. Followed by two annealing phases of 135 ºC for 4 minutes and 180 ºC for 3 minutes, respectively.

A 350 µL volume of a Protective Coating AR-PC 5090.02 (Electra 92) was subsequently spin-coated at 4000 RPM for 30 seconds and annealed at 150 ºC for 2 minutes.

A RAITH EBPG5150 100 kV e-BEAM Lithography System (EBL) was used to expose the desired structural designs on the PMMA layer.The EBL parameters and array dimensions of the designed samples can be found in Annex A.

Following exposure, the samples were developed. They were initially placed onto a beaker containing ultra-pure water (UPW) for 60 seconds to remove the conductive polymer. Afterwards, the samples were dried with N_2 gas and transferred inside a second beaker containing a MIBK:IPA solution, 1:3 ratio, for 90 seconds. Then, the samples were placed inside a third beaker containing only IPA for 90 seconds. A slight agitation was rendered using a tweezer when the samples were inside the beakers.

Afterwards, a BVR2008 FC Electron Beam Evaporator was used to deposit a 2 nm thick titanium layer, followed by a 50 nm thick gold layer. The sample was then left inside an acetone bath for 3 hours for lift-off.

The fabricated nanoparticles were characterized using a Scanning Electron Microscope (SEM) ZEISS Sigma and an Atomic Force Microscope (AFM) ICON Bruker to probe the quality of the particles and their height, respectively.

Then, a 150 nm organic blend layer of PDPPT5T:IEICO-4F [46] was spin-coated onto the sample containing the Au nanodisks structures.

3.3. **Solar cells fabrication and characterization**

Two samples were prepared to fabricate full solar cells. Each sample, contained four active regions where the nanostructured solar cells were fabricated.

To start, a glass substrate with ITO was cleaned, as described before. Then, a 10-minute 600W UV plasma cleaning process was performed in PVA TePla ION WAVE 10, before coating the samples with PMMA and the Protective Coating AR-PC, as described before.

EBL was used to expose the optimized patterns. The dimensions of the exposed arrays for each sample, as well as the dose and current, can be found in Annex A Table 6.

Next, a gold layer was deposited as described above. A layer of ZnO and PDPP5T:IEICO-4F [46] were spin-coated using the parameters of Table 1.

The top layers of MoO_3 and Ag were deposited using metal evaporation to achieve a thickness of 10 and 100 nm , respectively.

Lastly, after a 15 minute UV light exposure, the characteristic J-V curves were traced and external quantum efficiency measurements were carried.

Table 1 - ZnO and Organic blend spin coat parameters for full solar cell devices.

	Spin-coating		**Annealing**	
	RPM	Time (s)	Temp. (°C)	Time (min)
ZnO	4000	60	150	5
Organic Blend	720	60	-	-

4. RESULTS AND DISCUSSION

The simulations and fabrication results regarding the full solar cell device Jsc optimization and the strong coupling optimization in metallic structured semi-devices are presented in this section. The organic system used to incorporate the organic solar cells is PDPPT5T:IEICO-4F, which is an industry standard donor-acceptor blend. This blend allows for energy absorption within the visible and infrared energies of the spectrum - IR blend - which is most valuable for photovoltaics applications, considering the solar radiation spectrum.

4.1. FDTD Simulations

Numerical FDTD simulations are a powerful tool to optimize the geometrical parameters of optoelectronic devices. Two distinct structures were simulated: a full solar cell device and simpler device structures to investigate strong-coupling between surface lattices resonances and organic excitons of PDPPT5T:IEICO-4F. The structure of the full simulated devices, with and without gold nano particle lattices, is presented in Figure 4.1.

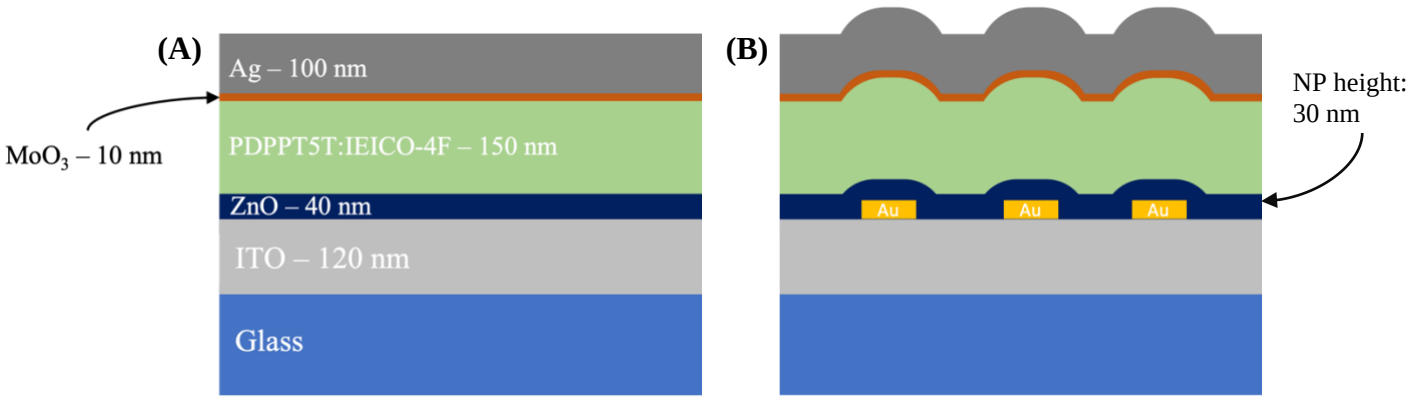

Figure 4.1 - Illustrative cross section of the simulated full solar cell structures. (A) a typical solar cell structure without the nanostructured lattice and (B) a solar cell cross section containing Au nanoparticle arrays.

To optimize the parameters of the structure in Figure 4.1(B) in order to achieve a short-circuit current enhancement, a particle swarm optimization (PSO) was carried out.[1] Through multiple generations and populations, the fitness parameter is updated towards its maximum value, corresponding to the maximum Jsc. Figure 4.2 illustrates the optimization of the fitness parameter, where the Y-axis represents the different populations, X-axis represents the different generations for each population and the color scheme indicates the value of short-circuit current for a nanostructured solar cell - FoM.

[1] The PSO was implemented by P. Bai, from the Applied Physics Department of Eindhoven University of Technology.

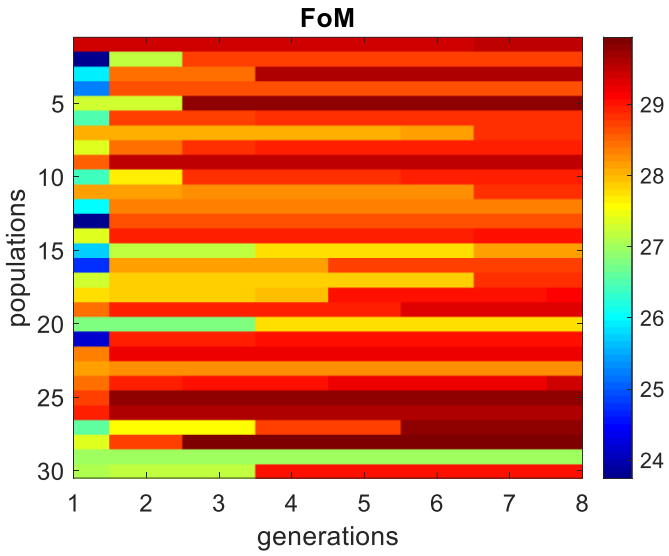

Figure 4.2 - Particle Swarn Optimization (PSO) of a metallic lattice nanostructured organic solar cell parameters values (metallic lattice diameter and pitches, and organic blend layer height). The optimizations consisted of 30 populations, represented in the Y-axis, over 8 generations, represented in the X-axis, aiming to achieve the highest fitness parameter value (short-circuit current) represented by the color diagram.

The highest Jsc value is attained for the 5th population in the 3rd generation, where the organic blend height is 76 nm and the nanoparticle lattice diameter and pitch are 100 and 331 nm, respectively. The short-circuit current, in this case, is 29.95 mA/cm2.

For a non-structured reference solar cell device - Figure 4.1(A) - a short-circuit current of 26.08 mA/cm^2 was calculated to be compared with the optimized design cell, where an approximately a 15 % enhancement it is achieved.

The complexity of this multilayered structure makes it difficult to probe the influence of the nanoparticle diameter and lattice pitch on SLRs, as well as on the strong coupling to the excitonic states of the organic blend. In this complex structure, the metallic lattice is surrounded by ZnO, which might reduce strong coupling effects. Thus, relatively simpler structures were simulated as depicted in Figure 4.3.

First, the structure on Figure 4.3(A) was simulated, where a nanoparticle is placed on a glass substrate, surrounded by a 150 nm thick medium. The purpose of this medium was to emulate the bare cavity, for which there is no absorption component due to excitons. Through the n and k (refractive index and extinction coefficient, respectively) optical constant values of the organic blend - Annex B - it is possible to choose the most adequate refractive index when k = 0, which for this case was 1.96.

Figure 4.4 illustrates the influence of the nanoparticle diameter and lattice pitch on the SLRs. For each example in Figure 4.4, the donor and acceptor extinction spectra is plotted in red and blue, respectively, as well as the surface lattice resonance extinction in black. Note that the extinction is defined as 1- Transmission,

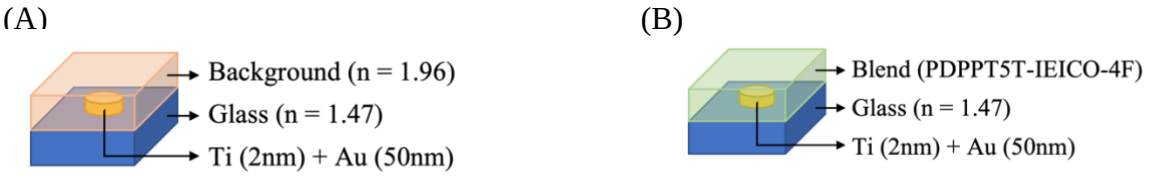

Figure 4.3 - Finite-Difference Time-Domain (FDTD) simulation schematics to (A) study the influence of diameter and pitch parameters on surface lattice resonance wavelengths, where a nanoparticle was placed on top of a glass substrate surrounded by a homogeneous medium emulating the PDPPT5T:IEICO-4F bare cavity and (B) to observe the emergence of polariton states resulting from the surface lattice resonance coupling to the organic exciton states of the blend layer.

corresponding to the absorbed and/or scattered fraction of the incident light - Annex C - where the transmission of the glass substrate used was taken as reference.

In Figure 4.4(A) the diameter (D) and pitch (P) of the simulated metallic lattice is 70 nm and 160 nm, respectively (D70 P160), whereas in Figure 4.4(B) the values of D and P are 100 nm and 270 nm (D100 P270) and lastly, in Figure 4.4(C) the D and P values are 130 nm and 355 nm (D130 P335). By adjusting the diameter and pitch, it was possible to tune the SLRs resonance.

By increasing the parameter values from D70 and P160 nm (Figure 4.4(A)) to D130 and P335 nm (Figure 4.4(C)) we can observe a clear redshift of the SLRs wavelengths from approximately 660 nm to 850 nm, respectively. In this work, the SLRs were purposefully tuned to overlap the PDPPT5T:IEICO-4F donor extinction spectra (Figure 4.4(A)), the acceptor extinction spectra (Figure 4.4(C)) and both simultaneously (Figure 4.4(B)), to achieve strong coupling between the SLRs modes and the organic blend exciton modes.

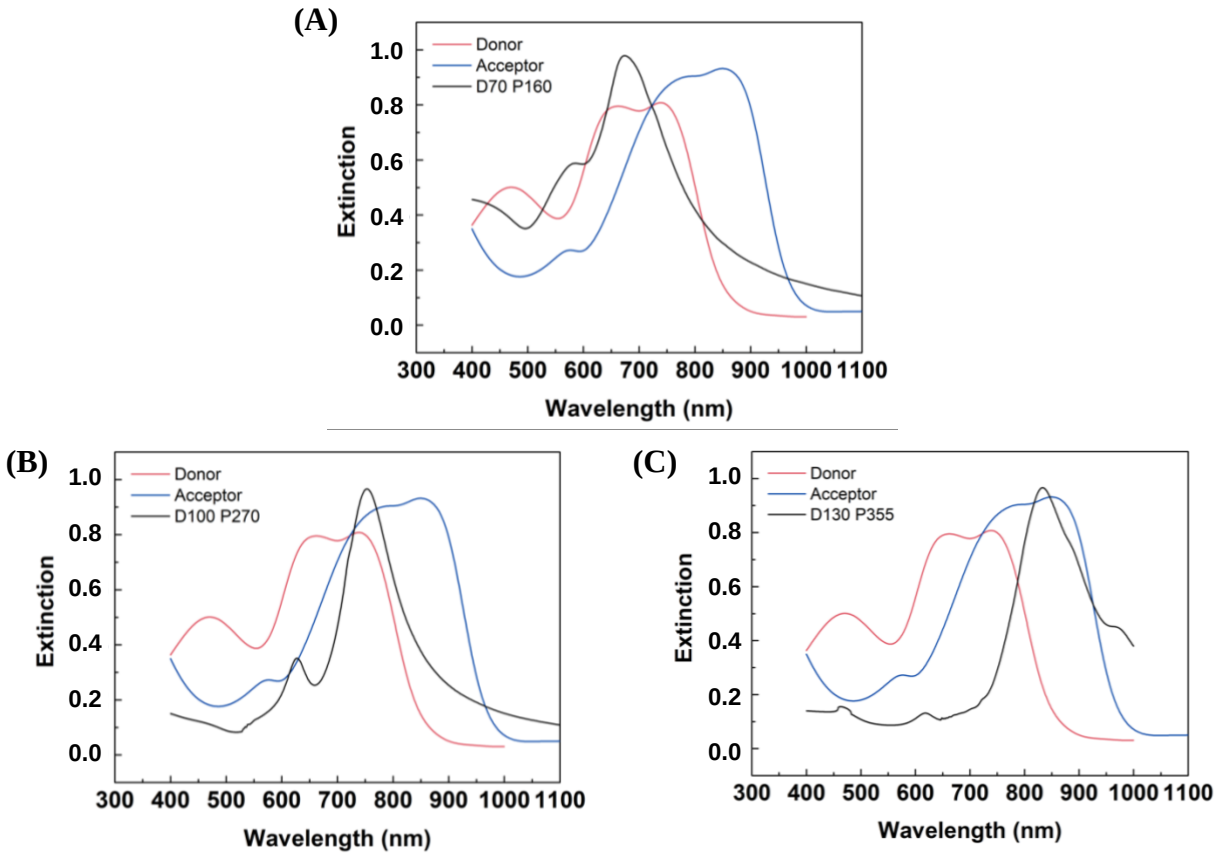

Figure 4.4 - FDTD extinction simulation results of PDPPT5T:IEICO-4F organic blend donor layer (in red), acceptor layer (in blue) and surface lattice resonances (SLRs) arising from gold nanodisk lattices (in black). The diameter (D) and pitch (P) of the SLRs are (A) 70 and 160 nm, (B) 100 and 270 nm and (C) 130 and 335 nm, respectively. By shifting the diameter and pitch, it is possible to achieve different SLRs wavelengths. In this work, the SLRs were tailored to overlap the PDPPT5T:IEICO-4F: (A) donor, (B) in-between donor and acceptor and (C) acceptor spectra regions.

The donor (PDPPT5T) and acceptor (IEICO-4F) of the organic blend layer collectively absorb light within a wavelength range of 600-900 nm as depicted in Figure 4.4, thus being considered an infrared organic blend. This type of organic blend is quite favorable for OPV technology since the highest solar irradiance wavelengths match with the PDPPT5T- IEICO-4F absorption wavelength range. In addition, this blend is also semi-transparent in the visible region, allowing to be further exploited in novel OPV technologies, e.g., solar cells integrated in windows.

Subsequentially, the structured depicted in Figure 4.3(B) was simulated. The material constants (n and k values) obtained experimentally through ellipsometry measurements were used to simulate the extinction of organic blend layer surrounding the particle array, resulting in Figure 4.5(A) black curve. By adding the

organic blend layer to the system, polariton states arise from the coupling of surface lattice resonances with the excitonic states of matter of the organic blend.

In Figure 4.5(B), the presence of these hybrid states can be seen (in red), as they modify the extinction spectra. The formation of two shoulders at approximately 600 and 950 nm indicate the presence of the polariton states. Moreover, by observing the extinction ratio (ΔE) of the normalized coupled system spectra with respect to the organic blend spectra, it is possible to have a clearer view over both the upper and lower polaritons established by the strong coupling, Figure 4.5(C).

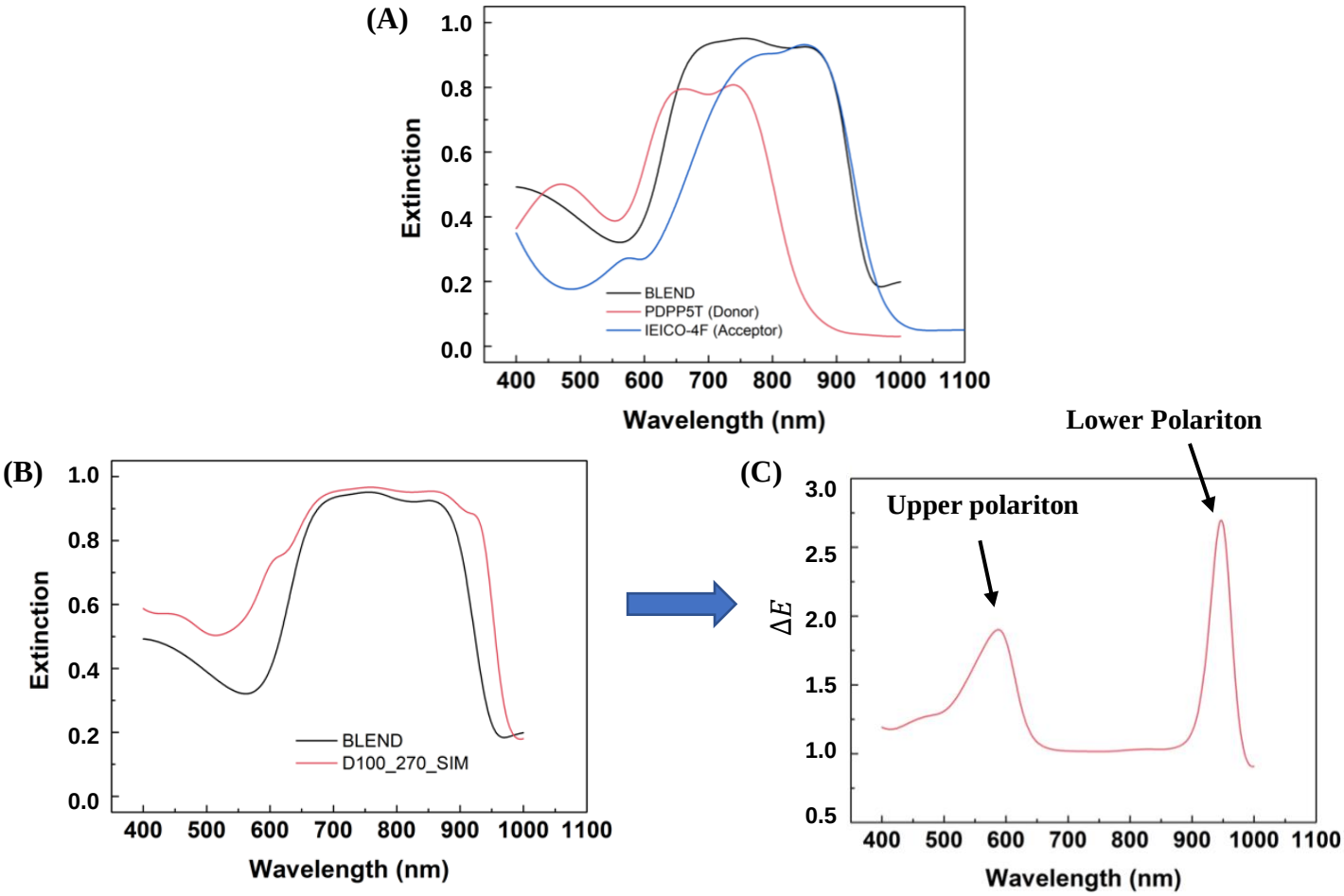

Figure 4.5 - FDTD extinction simulations results of (A) PDPPT5T:IEICO-4F organic blend (in black) with the respective donor (in red) and acceptor layer (in blue), (B) PDPPT5T:IEICO-4F extinction spectra (in black) compared to strongly coupled system of PDPPT5T:IEICO-4F organic excitons and SLRs emerging from gold nano disk lattices with a diameter of 100 nm and a pitch of 270 nm (in red) with two visible shoulders at approximately 600 and 950 nm, and (C) the extinction ratio (ΔE) of the normalized coupled system spectra with respect to the organic blend spectra.

The figures presented so far are illustrative examples of the several cases which were studied to achieve strong-light matter coupling between the SLRs and the donor and acceptor layers, either individually or simultaneously. Considering the several values of diameters and pitches, achieved through simulations, to optimize the coupling strength, only six pairs of values were chosen to fabricate samples - Table 2.

Table 2 - Au NPs optimized diameter and pitch values for the considered scenarios.

Scenarios	**SLR - Donor couple**		**SLR - Donor and Acceptor couple**		**SLR - Acceptor couple**	
Diameter (nm)	70	70	100	120	130	150
Pitch (nm)	120	160	270	240	335	420

4.2. **Au nano particle arrays**

To study and characterize simpler gold nanoparticle array structures to gain insight on strong light-matter coupling established between SLRs and excitons in acceptor-donor blends, samples of glass substrate with nano disk arrays on top were prepared as described in chapter 3.2.

The layout of this sample was designed anticipating experimental errors induced during the fabrication. - Figure 4.6. For each diameter value presented in Table 2, four arrays of particles were designed, starting from the initial value, further decreasing it in steps of 5 nm (in black). For these structures a 2 nA beam current was used in EBL.

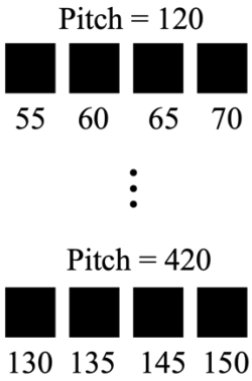

Figure 4.6 - Metallic nano particle lattices sample layout, containing four test arrays for each diameter.

Before coating the sample with PDPPT5T-IEICO-4F blend, a 300 nm thick layer of polysterine was spin coated. Polysterine has a refractive index of 1.6 [47] which is fairly close to the simulated bare cavity layer refractive index of 1.96. Thus, it was possible to experimentally measure the optical response of the SLRs uncoupled states on the sample.

Subsequentially, the polysterine layer was removed with anhydrous chloroform, and a 150 nm layer of the organic blend layer was spin coated onto the sample to retrieve optical measurements of the PDPPT5T-IEICO-4F blend and the coupled states of SLRs and organic excitons.

The following results present the spectrometry measurements of the nanostructured lattice uncoupled SLRs and the measurements of the coupled states between the resonances and the organic excitons.

Figure 4.7 illustrate the SLRs, emerging from metallic nano disks with a diameter (D) of 70 nm and a pitch (P) of 160 nm, designed to overlap with the donor layer spectra of the PDPPT5T-IEICO-4F organic blend (around 700 nm wavelengths). Figure 4.7(A) shows the experimental uncoupled organic blend (in black) and SLR (in red). The noise present in the uncoupled SLR measurements is due to misalignments in the spectrometry system, however it does not affect the visibility of the SLR peak. Figure 4.7(B) shows the spectrometry measurements of lattices surrounded by the organic blend layer. Lastly, Figure 4.7(C) shows the extinction ratio (ΔE) of the normalized SLR:blend system spectra with respect to the organic blend spectra.

Figure 4.7(B) and (C) might lead to believe the SLR is coupled to PDPPT5T-IEICO-4F organic blend, resulting in the peak approximately at 560 nm. Nevertheless, the uncoupled states, in Figure 4.7(A), show that the emergent peak results from the addition of the individual SLR and the organic blend extinction spectras and not from the coupling between the two states.

Figure 4.7(D) SEM images show spherical nano disks which appear to be well defined. Attending to the fact that the substrate is non-conducting, it was difficult to achieve clear images due to charging effects, even when a sample holder with a copper clamp was used. The diameters and pitches of the nano disks were retrieved using ImageJ Software - by averaging several nanoparticle diameter values, it was possible to attain a more representative value. Although the desired diameter for these lattices was 70 nm, experimental measurements show a diameter of 83 nm. The second set of metallic lattices with a diameter of 70 nm and a pitch of 120 nm, also intended to overlap the donor spectra of the organic blend, displayed similar spectrometry results.

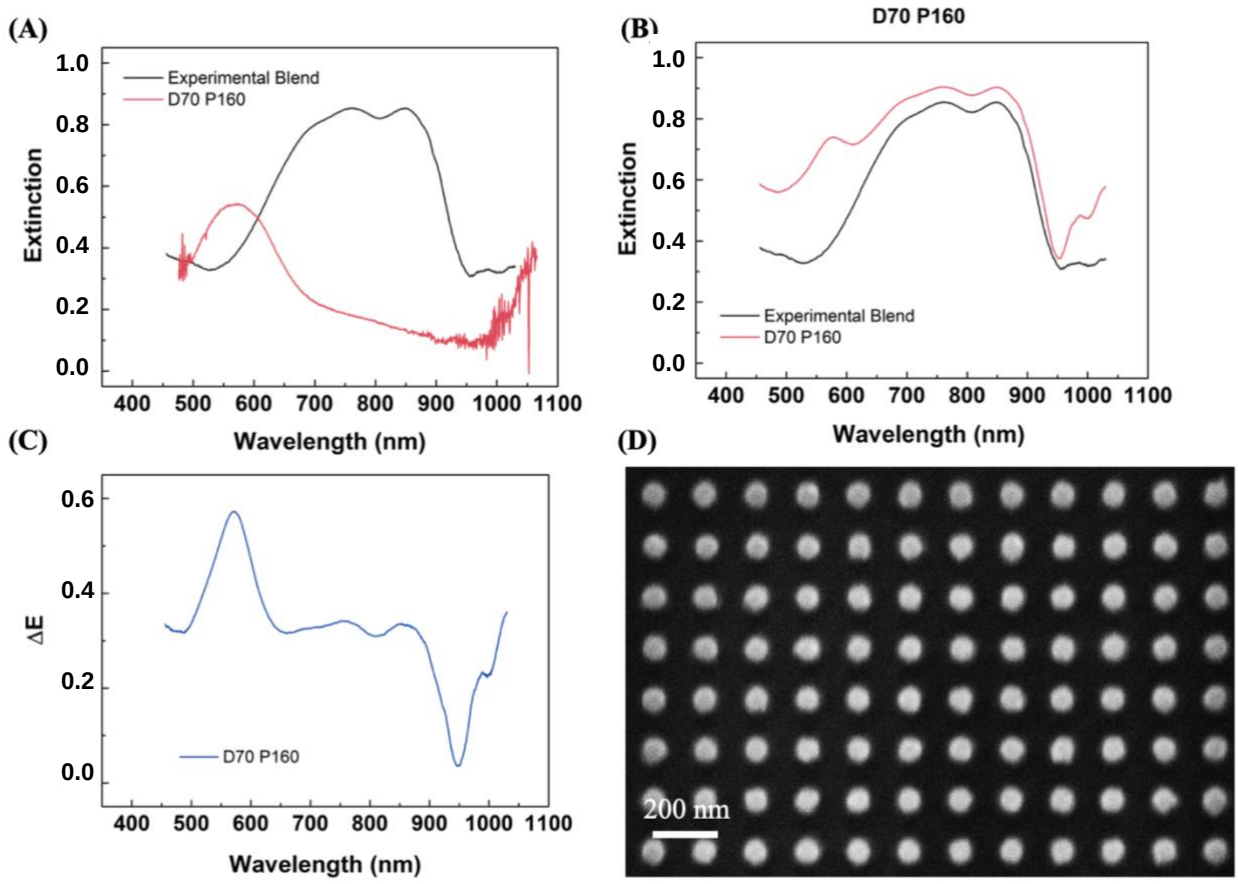

Figure 4.7 - Spectrometry extinction results of (A) uncoupled states of SLRs emerging from gold nano disk lattices with a diameter of 70 nm and a pitch of 160 nm (in red) measured in 300 nm thick medium with n=1.6 and PDPPT5T:IEICO-4F organic blend (in black), (B) SLRs plus PDPPT5T:IEICO-4F system (in red) and organic blend (in black), (C) the extinction ratio of the normalized spectra of the SLRs plus PDPPT5T:IEICO-4F system (in blue), with respect to the organic blend. (D) SEM images of gold nano disk lattices with 70 nm in diameter and 160 nm in pitch.

In Figure 4.8, the SLR arising from metallic nano disks, with diameter (D) of 120 nm and pitch (P) of 240 nm was designed to overlap simultaneously the donor and acceptor layer spectra of the PDPPT5T-IEICO-4F organic blend. In Figure 4.8, panel (A) shows the experimental uncoupled organic blend (in black) and the SLR (in red), panel (B) shows the spectrometry measurements of lattices surrounded by the organic blend layer and panel (C) shows the extinction ratio (ΔE) of the normalized SLR:blend system spectra with respect to the organic blend spectra and panel (D) shows SEM images of the metallic lattices.

It is clear, by Figure 4.8(A), that the SLR is not overlapping both the donor and acceptor layers of the organic blend as intended. In fact, the SLR is not coupling to either donor or acceptor, and the peak present approximately at 625 nm in Figure 4.8(B), results, once more, from the addition of the uncoupled states extinction spectra. Thus, the enhancement of the extinction spectra present in Figure 4.8(C), near 625 nm is caused by the SLR spectra and not by the presence of hybrid states. On the other hand, the metallic lattices, in

Figure 4.8(D), presented an experimental diameter of 123 nm, which is excellent, considering the desired diameter of 120 nm.

Similar results were obtained for the alternative SLR, emerging from lattices with 100 nm in diameter and 240 nm in pitch, which was also expected to overlap both donor and acceptor layer of the PDPPT5T-IEICO-4F organic blend.

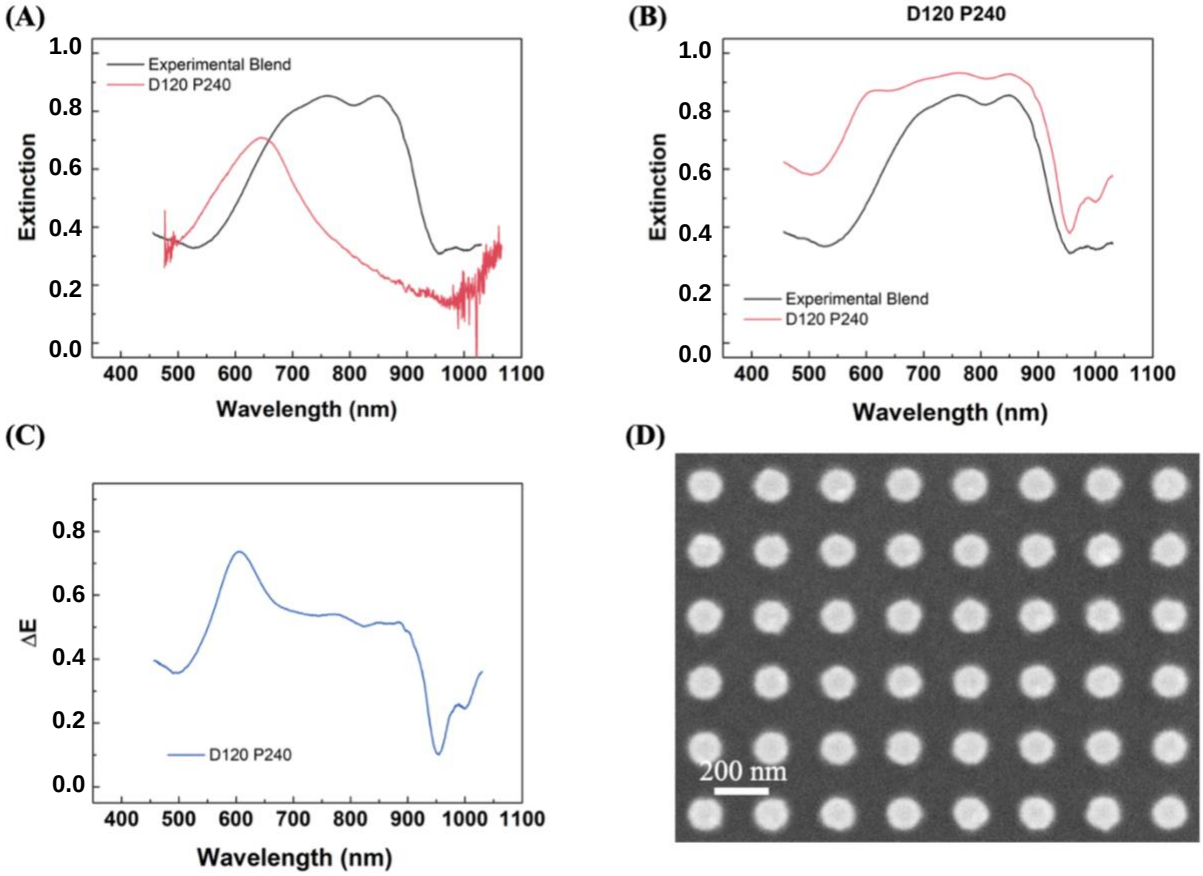

Figure 4.8 - Spectrometry extinction results of (A) uncoupled states of SLRs emerging from gold nano disk lattices with a diameter of 120 nm and a pitch of 240 nm (in red) measured in 300 nm thick medium with n=1.6 and PDPPT5T:IEICO-4F organic blend (in black), (B) SLRs plus PDPPT5T:IEICO-4F system (in red) and organic blend (in black), (C) the extinction ratio of the normalized spectra of the SLRs plus PDPPT5T:IEICO-4F system (in blue), with respect to the organic blend. (D) SEM images of gold nano disk lattices with 120 nm in diameter and 240 nm in pitch.

Figure 4.9 shows the results of the SLR originated from a 130 nm in diameter (D) and 335 nm in pitch (P) gold nano disk lattice. Panels (A), (B), (C) and (D) of Figure 4.9 illustrate the same type of measurements mentioned for the previous cases. The SLR (in red), presented in Fig.11(A), was initially designed to exclusively overlap the acceptor layer spectra of the organic blend (near 850 nm wavelengths).The experimental data shows two peaks at approximately 530 and 750 nm. The smaller peak corresponds to the 1st order Rayleigh anomaly (RA) and can be calculated through $RA = n \times a$, where n is the refractive index of the particle surrounding medium and a is the lattice pitch. In this case $RA = 1.6 \times 335 = 536\,nm$. Interestingly, the second peak (at 750 nm) overlaps both donor and acceptor layers extinction spectra. In Figure 4.9(B), it is clear the emergence of a peak at approximately 950 nm. Unlike previous cases, this peak resulted from the coupling of the SLR and the PDPPT5T-IEICO-4F exciton states - polariton peak. By normalizing the extinction of this coupled system, with respect to the organic blend, it is possible to have a clearer view over the formation of these peaks. The normalized spectra of the coupled system - Figure 4.9(C) - not only shows the lower polariton peak at 950 nm, but also allows to observe the presence of a second peak at approximately 650 nm - upper polariton peak - which is not distinguishable through Figure 4.9(B). Figure 4.9(C) is quite similar to the simulated results of Figure 4.5(C), where two polariton peaks are clearly visible

Lastly, the experimental diameter of the lattice present in Figure 4.9(D) is 151 nm, which is higher than the expected 130 nm.

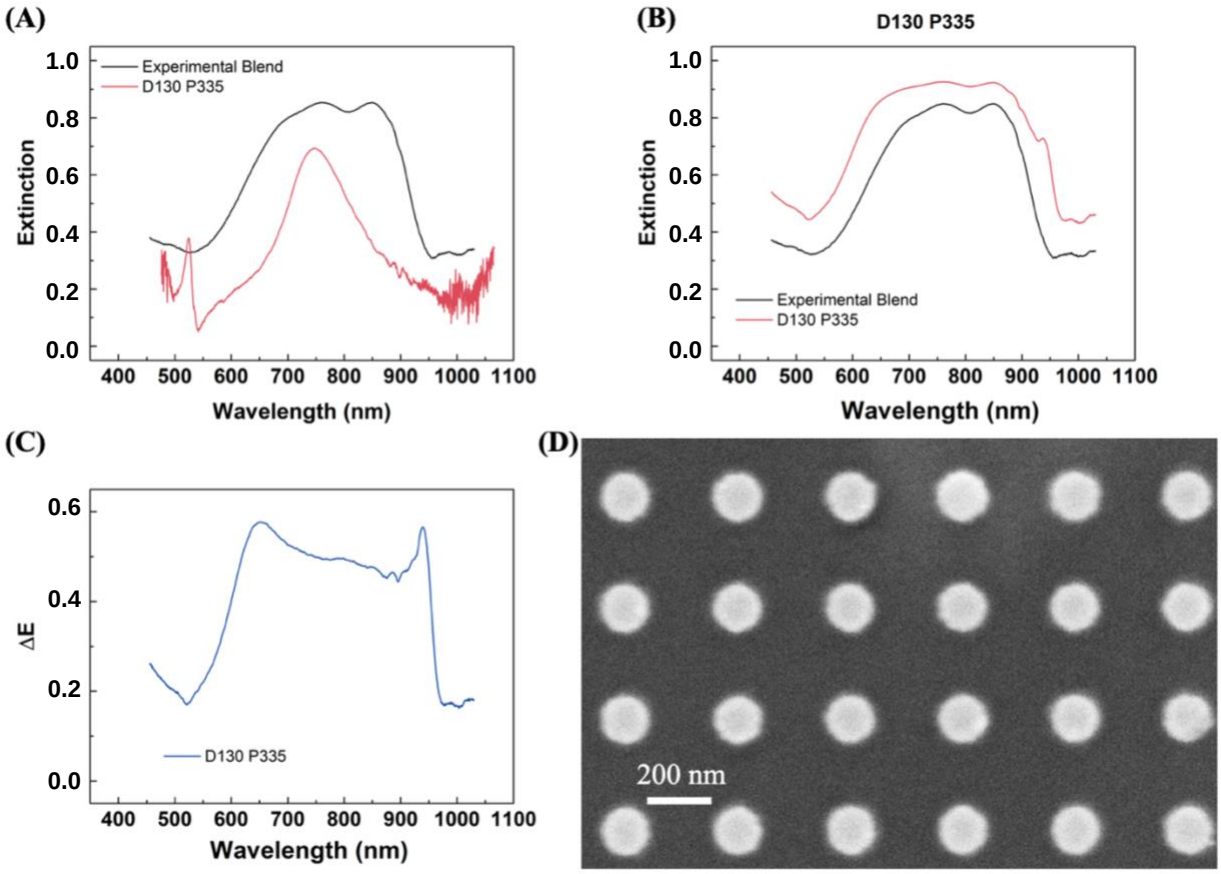

Figure 4.9 - Spectrometry extinction results of (A) uncoupled states of SLRs emerging from gold nano disk lattices with a diameter of 130 nm and a pitch of 335 nm (in red) measured in 300 nm thick medium with n=1.6 and PDPPT5T:IEICO-4F organic blend (in black), (B) SLRs plus PDPPT5T:IEICO-4F system (in red) and organic blend (in black), (C) the extinction ratio of the normalized spectra of the SLRs plus PDPPT5T:IEICO4-F system (in blue), with respect to the organic blend. (D) SEM images of gold nano disk lattices with 130 nm in diameter and 335 nm in pitch.

The results of the alternative metallic lattice, with a diameter of 150 nm and a pitch of 420 nm, of which SLR was designed to overlap with the acceptor layer of the organic blend, is present in Figure 4.10. The SLR at approximately at 800 nm, emerging from Figure 4.10(D) structures, does not exclusively overlap the PDPPT5T:IEICO4-F acceptor layer, as intended - Figure 4.10(A). Nevertheless, the coupling of the organic blend excitons with the SLR results in the emergence of a peak at approximately 960 nm, as seen in Figure 4.10(B). The normalized coupled system, with respect to the organic blend - Figure 4.10(C) - shows the lower polariton peak, at 960 nm and a faint lump at approximately 650 nm. The latter, could indicate the upper polariton peak, however, the broad spectra of the PDPPT5T:IEICO-4F organic can mask the presence of well-defined peaks. An additional peak was also observed in Figure 4.10(A), at approximately 600 nm. Since the 1st order RA for this lattice is around $1.6 \times 420 = 672\ nm$, this peak likely is the localized surface plasmon resonance (LSPR) of a single nano particle.

Lastly, the SEM image, Figure 4.10(D), of the lattices show an experimental diameter of 174 nm, which is higher than the intended diameter of 150 nm.

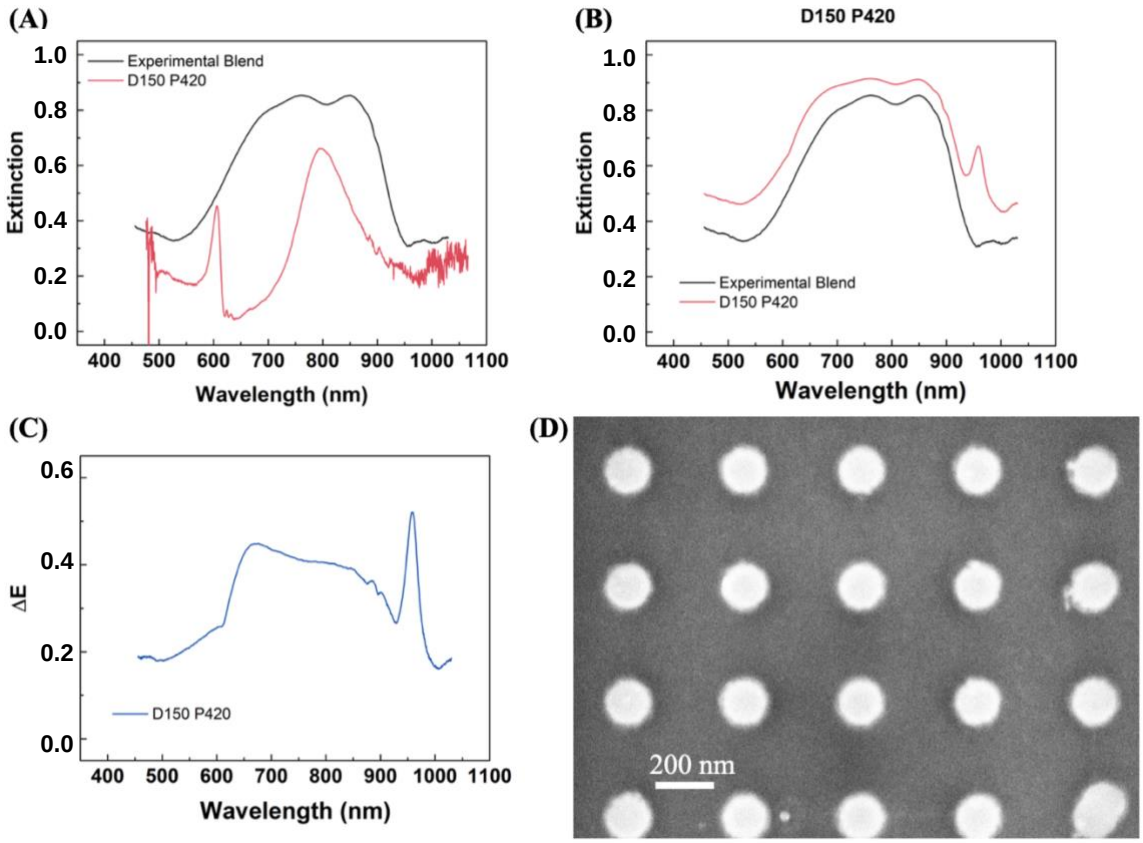

Figure 4.10 - Spectrometry extinction results of (A) uncoupled states of SLRs emerging from gold nano disk lattices with a diameter of 150 nm and a pitch of 420 nm (in red) measured in 300 nm thick medium with n=1.6 and PDPPT5T:IEICO-4F organic blend (in black), (B) SLRs plus PDPPT5T:IEICO-4F system (in red) and organic blend (in black), (C) the extinction ratio of the normalized spectra of the SLRs plus PDPPT5T:IEICO4-F system (in blue), with respect to the organic blend. (D) SEM images of gold nano disk lattices with 150 nm in diameter and 420 nm in pitch.

The following table summarizes the designed and the respective experimental diameter values for the metallic lattices presented above:

Table 3 - Summary table of diameter dimensions of the most promising Au NPs arrays.

Arrays	**Diameters (nm)**					
Designed	70	70	100	120	130	150
Experimental	81	83	104	123	151	174

By observing Table 3, it is possible to see that for the diameters of 100 and 120 nm, the experimental diameter corresponds perfectly to the designed one. These arrays were fabricated with a 10 nm difference with respect to the designed value. Further analysis of the arrays showed that to process nanoparticles with a specific diameter, it is ideal to offset the designed diameter value predominantly by 10 nm, except for higher diameters, such as 130 and 150 nm, where the optimal offset is 15 nm.

Having the full solar cell device fabrication in mind, three of the most promising arrays were selected from Table 3 to be incorporated later in solar cells, these being the metallic lattices with diameter (D) and pitch (P) values of: D70 P160 nm, D130 P335 nm and D150 P420 nm. Both D=130 and D=150 nm lattices were selected since they present IR enhancements. This is the most interesting region to optimize the absorption of the cell since it coincides with the highest solar irradiance wavelengths.

To evaluate the power absorbed by the gold nanostructures and the organic blend, a *Pabs_advanced* box was used in ANSYS Lumerical, comprising the organic blend layer and gold nanostructures. Figure 4.11 illustrates the simulations of the power absorbed per unit of volume, normalized in respect to the source power, for the Au nanoparticle (in red), the organic blend (in black) and the total power absorption (in blue).

By comparing the Au NP and blend absorption spectra, it is clear that the latter does not play a major role when it comes to enhancing the absorption of the overall device. However, the gold nanodisks present clear absorption peaks for the arrays with nanoparticles with D=130 (Figure 4.11(B)) and D=150 nm (Figure 4.11(C)) approximately at 960 and 1020 nm, respectively. As for the Au NPs with D=70 nm - Figure 4.11(A), there is no evidence of a clear peak unlike the previous cases, however there is an increase of power absorption near 560 nm, creating a visible lump on total absorption curve (in blue) which matches with the SLR peak in Figure 4.7(A).

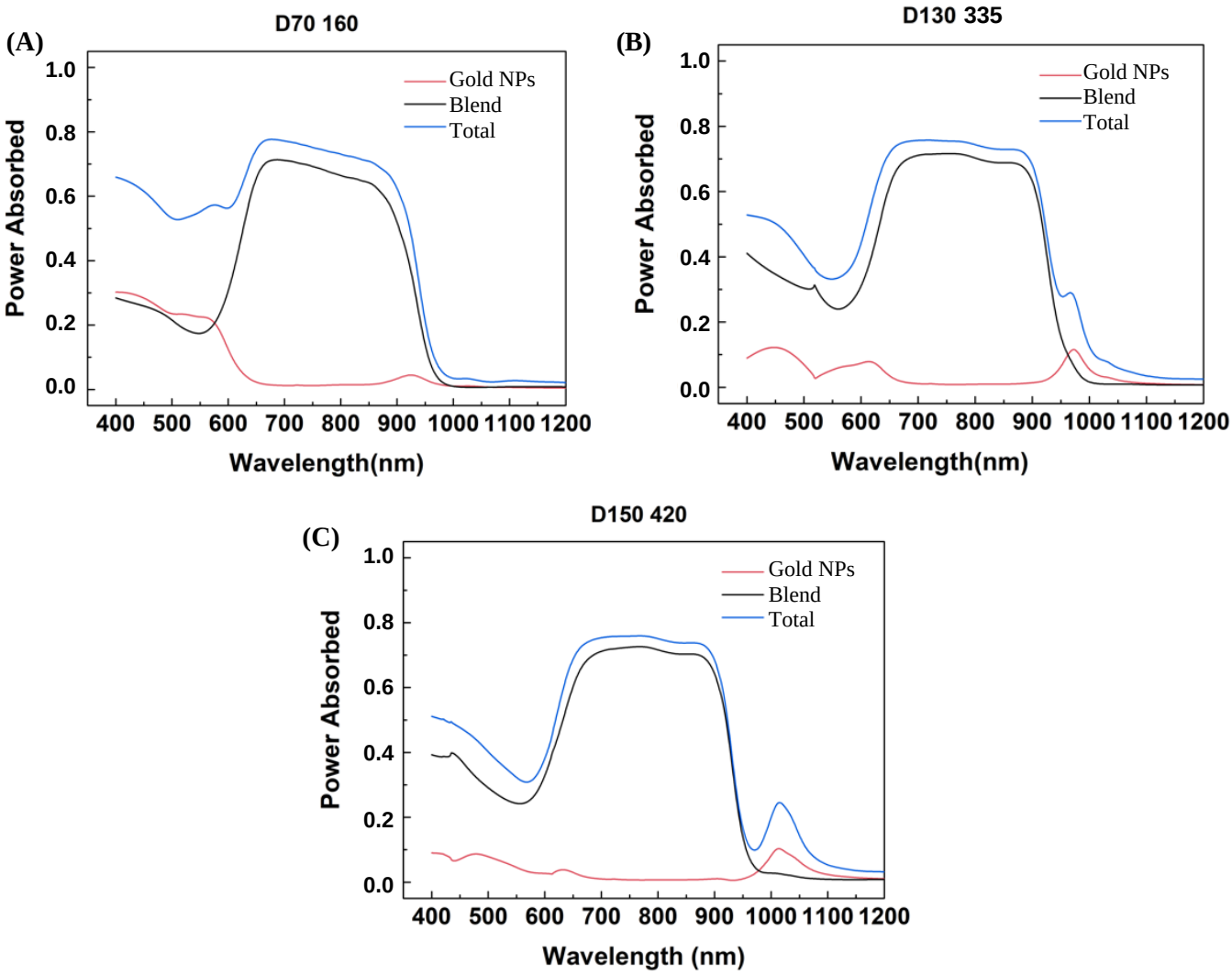

Figure 4.11 - FDTD simulations of the power absorbed per unit of volume, normalized to the source power, within the PDPPT5T:IEICO-4Forganic blend layer placed on top of nanoparticle arrays. The individual absorption of the organic blend is depicted in black, the gold nanoparticle lattice absorption in red and the total absorption in blue for lattices with (A) 70 nm particle diameter and 160 nm pitch, (B) 130 nm particle diameter and 335 nm pitch and (C) 150 nm particle diameter and 420 nm pitch.

Additional measurements were done in a Fourier microscopy setup, to infer the extinction dispersion of the lattices. Fourier microscopy is an important tool to characterize optical nanostructures. This type of microscopy allows to quantitatively measure information about the angular spectra of a microscopic sample. The setup used in this work can be found in Annex D. The following example illustrates the Fourier results obtained for a lattice with nanoparticles of 130 nm diameter and a pitch of 335 nm - where the SLRs energy

was intended to overlap the organic blend acceptor layer extinction. In this diagram, the Y-axis represents the photon energy, in eV (left) and wavelength (right), and the X-axis ($K_{//}$) is the parallel wavevector to the surface of the incident plane wave, define as $\frac{2\pi}{\lambda}\sin(\theta)$, where θ represents the incident angle measured with respect to the surface normal. The color scale represents the extinction of the sample. Figure 4.12(A) and Figure 4.12(B) are the extinction dispersion of the same sample, measured for transverse magnetic (TM) and transverse electric (TE) polarization, respectively, normalized with respect to the extinction of a layer of PDPPT5T:IEICO-4F organic blend.

In Figure 4.12, two distinct Rayleigh anomalies can be observed for (+1,0) and (-1,0) diffraction orders - dashed yellow lines in Figure 4.12(A). Additionally, two vertical lines can be noticed in both measurements of Figure 4.12 that could not be explained. A noticeable shift in energy can be seen, as the lower polariton energy band depicted by the dark grey dots bends, shifting from wavelengths of approximately 900 nm, Figure 4.12(A), towards lower energies, at approximately 950 nm (Figure 4.12(B)) - in accordance to the spectrometry results in Figure 4.9(C). Additionally, a faint energy band (in light orange), can be observed at 650 nm, resembling the peak seen in Figure 4.9(C).

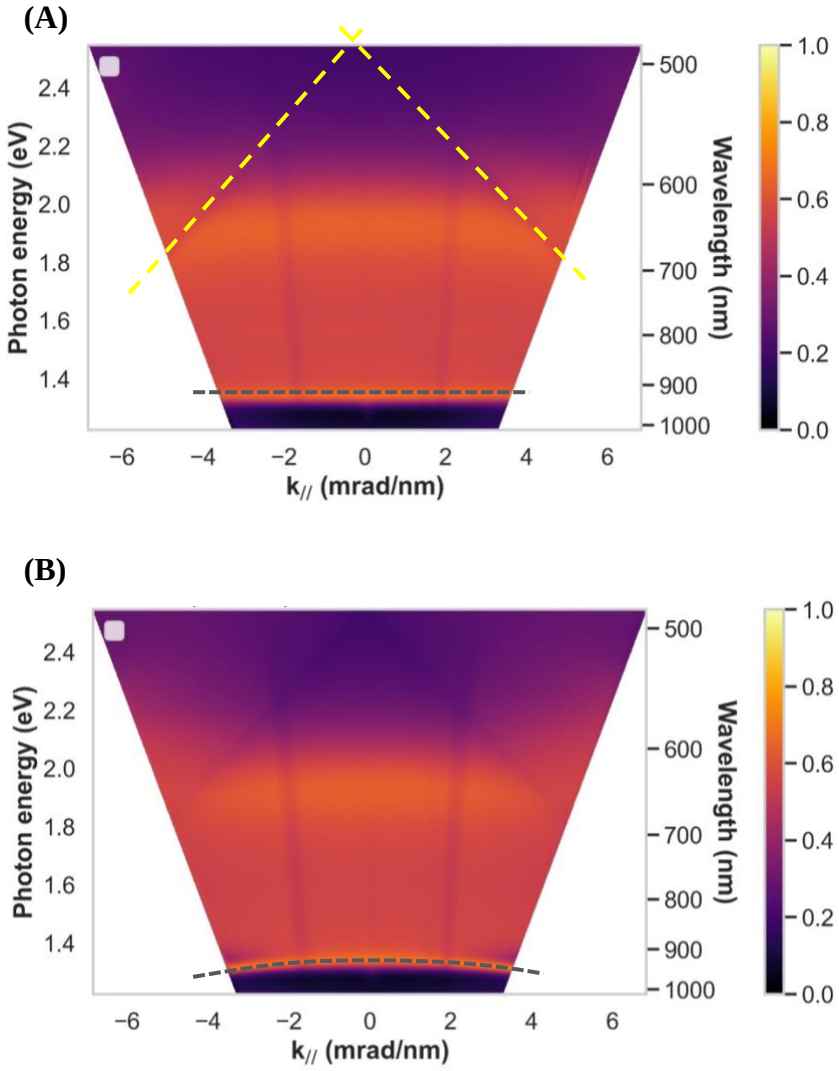

Figure 4.12 - Fourier measurements of extinction dispersion for metallic arrays with 130 nm in diameter and 335 nm in pitch under (A) Transverse Magnetic and (B) Transverse Electric polarizations, normalized with respect to a PDPPT5T:IEICO-4F organic blend layer.

4.3. **Solar cells devices**

Each full solar cell layout had four active areas where the devices were fabricated. Two of these regions had smaller areas of 0.09 cm^2, while the remaining two had bigger areas of 0.16 cm^2. For each sample, one cell was left with no arrays (as a reference), whereas the other three were designed to contain the arrays referred in Figure 4.11. Figure 4.13 illustrates the layout containing the active areas (in blue), the ITO bottom electrode contact (in light grey), and the Ag metal electrode contact (in dark grey) on a 0.5 mm grid.

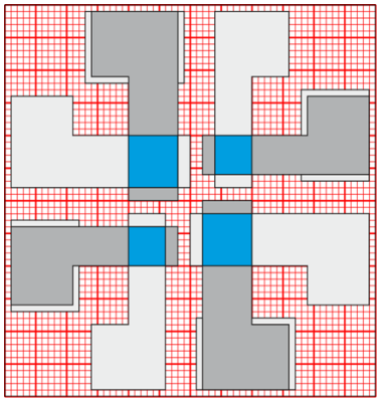

Figure 4.13 - Fabricated full solar cell device layout, containing four active regions in blue, connected by "L" shaped electrodes of ITO (dark grey) and Ag (light grey), behind a 0.5 mm grid, for reference.

Two samples were prepared[2], containing similar lattices. In sample A, the lattices were embedded in the ZnO layer whereas, in sample B, the arrays were deposited on top of the ZnO layer.

In sample A, the nanoparticle height was limited by the ZnO layer, which has a thickness of 40 nm, thus the fabricated gold structures were designed to have 30 nm in height, contrary to sample B, where there was no height limitation, therefore allowing the fabrication of 50 nm tall arrays. To acquire information about the experimental height and diameter of the fabricated nanoparticle arrays of the solar cells in sample A, AFM measurements were carried out - Figure 4.14.

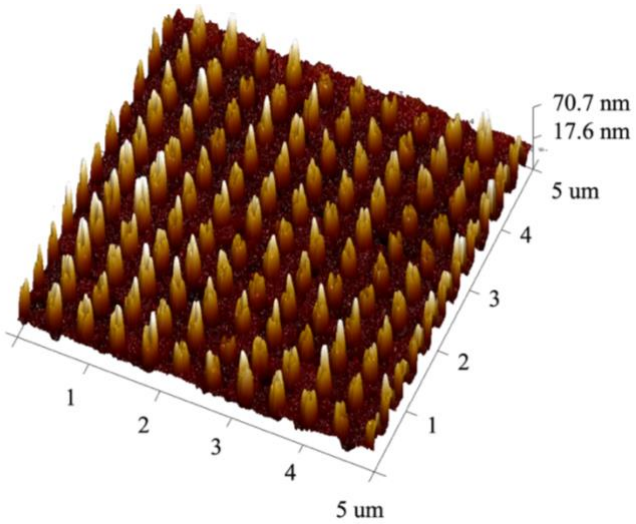

Figure 4.14 - Atomic force microscopy (AFM) image of a 5x5 μm metallic lattice region with 150 nm in diameter and 420 nm in pitch.

[2] In collaboration with T.P.A. Van der Pol from the Chemical Engineering and Chemistry Department of Eindhoven University of Technology.

The following table summarizes the AFM results for sample A heights and diameters.

Table 4 - AFM results for sample A solar cell array diameter and height.

	Projected		AFM	
	Diameter (nm)	**Height (nm)**	**Diameter (nm)**	**Height (nm)**
Sample A	70	30	78,17	38,83
	130	30	162,8	37,67
	150	30	174,5	37,17

The diameters measured with AFM on sample A presented some differences with the SEM results of Table 3, likely due to the inherent error associated with the AFM tips geometry.

The heights of the nanoparticle arrays, displayed in Table 4, also present some differences regarding the desired value of 30 nm - overall being almost 1/3 higher than expected. These differences can also be an artifact from the AFM tip geometry.

Following with the full device's fabrication, the samples were characterized regarding their J-V curves and EQE to probe their optical response[3]. The results of these two characterizations are shown from Figure 4.15 to Figure 4.17, as well as in Table 5, where all the relevant parameters, for each characterization, are summarized.

The J-V curves of the solar cells for sample A is illustrated in Figure 4.15. By comparing the reference cell (black curve) and the nanostructured cell (color curves) it is conclusive that there was not a short-circuit current enhancement - as it suffered a slight decrease in current due to the reflection of the incident light by the lattices.

It is worth mentioning that the lattices were simulated and designed in simpler structures with different surrounding mediums, adding to the complexity of layers in the final structure, strong coupling effects are mitigated. On the other hand, it is also observable that the nanostructured solar cells' Voc - approximately 0.54 V - is the same as the reference. These are very encouraging results since, among other factors, the solar cell morphology plays an important role regarding its Voc [10] and by incorporating nanoparticle arrays , and thus

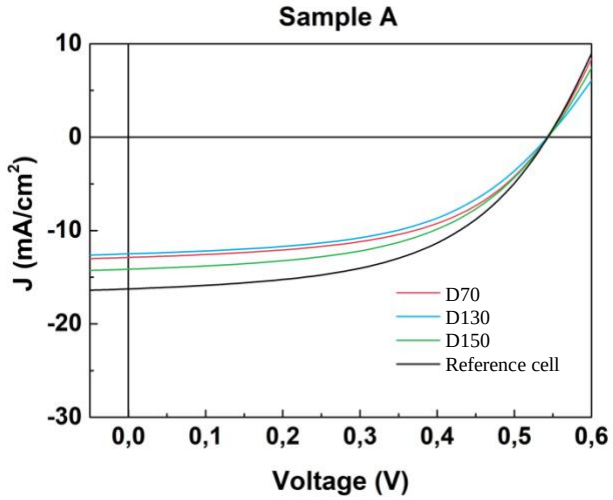

Figure 4.15 - J-V curves of sample A, illustrating the gold nano disk structured solar cells in color, with metallic lattices with diameters (D) and pitches (P) of: D70 P160 nm (in red), D130 P335 nm (in blue) and D150 P420 nm (in green) and the reference cell without arrays (in black).

[3] The JV curves and EQE measurements were performed with the assitance of T.P.A. Van der Pol from the Chemical Enginnering and Chemistry Department from Eindhoven University of Technology.

changing the device's morphology, no degradation was induced in the open-circuit voltage of the samples. The fill factor of the solar cells, power conversion efficiency, Jsc, and Voc were determined from the measurements and are given in Table 5. By taking a closer look, we see that the fill factor did not suffer oscillations, remaining approximately close to 0.51. Despite the steady Voc and FF, the conversion efficiency is still impacted by the Jsc of the cells, suffering a slight decrease.

Lastly, the J-V curves of sample B (not shown) revealed that every nanostructured cell was short-circuited, thus demonstrating that it is not viable to deposit the gold nanoparticles above the ZnO layer.

Figure 4.16 shows the results for the external quantum efficiency of sample A. The dashed and solid lines in the Figure 4.16 represent the EQE measurements with and without bias, respectively. Comparing all nanostructured cells with Au lattices (in color) with the reference cell (in black), where no arrays were implemented, it is clear that the presence of these structures strongly influences the shape of the EQE spectra. Overall, the EQE of the structured cells is lower than the reference cell. However, a small enhancement can be noticed approximately at 580 nm, for the cell with D=130 nm (green curve). In addition, for cells with nanoparticles of diameter D=65 and D=130 nm , a noticeable shift of the absorption edge can be observed by zooming sample A spectra - Figure 4.17, indicating that metallic lattices can indeed be exploited in organic photovoltaics to reshape the absorption spectra towards higher enhancements. Considering that the Voc displayed no degradation by the incorporation of the lattices and that the Jsc suffered a slightly reduction due to the reflection of the arrays, I believe these are very promising results for further work regarding nanostructured OPV technology.

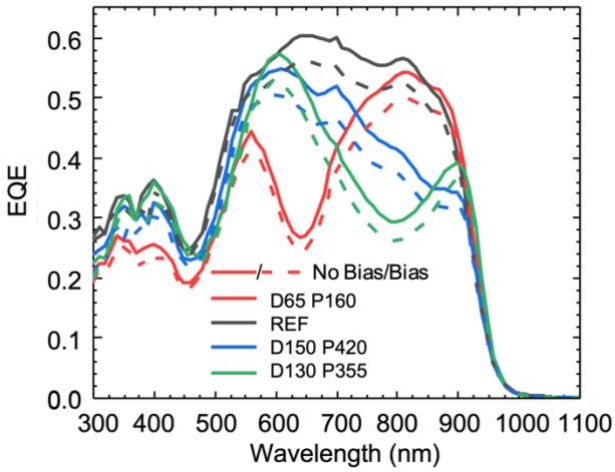

Figure 4.16 - External quantum efficiency (EQE) measurements of gold nano disk nanostructured organic solar cell, illustrated in color, with metallic lattices of 65 nm diameter (in red), 130 nm diameter (in green) and 150 nm in diameter (in blue) and the reference cell without arrays (in black). The solid lines represent the EQE measurements with no bias, whereas the dashed lines are relative to the measurements with bias.

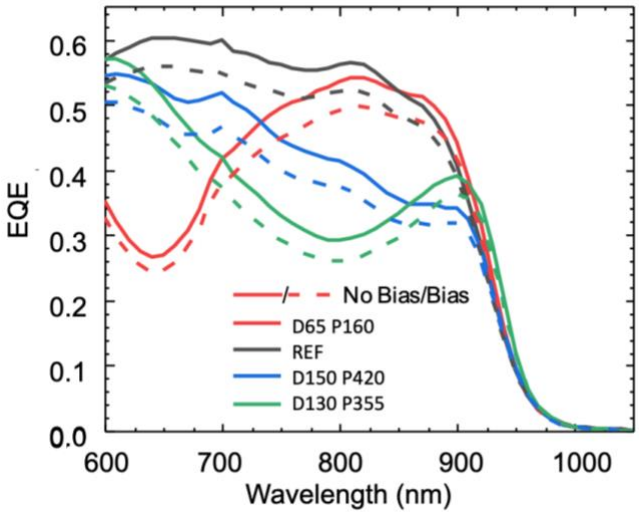

Figure 4.17 - Zoomed-in external quantum efficiency (EQE) measurements of gold nano disk nanostructured organic solar cell, illustrated in color, with metallic lattices of 65 nm diameter (in red), 130 nm diameter (in green) and 150 nm in diameter (in blue) and the reference cell without arrays (in black). The solid lines represent the EQE measurements with no bias, whereas the dashed lines are relative to the measurements with bias.

Table 5 - Summary table of J-V curves and EQE extracted parameters values.

Sample	Arrays	Jsc (mA/cm^2)	Voc (V)	FF	PCE	EQE nobias	EQE bias
A	REF	15.8	0.541	0.511	4.43	17.4	16.33
	D70 P160	11.7	0.548	0.444	2.8	13.62	12.64
	D130 P335	12.5	0.541	0.509	3.45	13.69	12.59
	D150 P420	13.7	0.543	0.503	3.75	14.75	13.55
B	REF	11.9	0.297	0.297	1.05	17.09	12.43
	D70 P160	-	-	-	-	-	-
	D130 P335	-	-	-	-	-	-
	D150 P420	-	-	-	-	-	-

5.
CONCLUSIONS AND FUTURE PERSPECTIVES

The goal of this work was to simulate, fabricate and characterize full solar cell devices to optimize the short-circuit current, as well as simpler structures to probe and maximize the strong light-matter coupling between surface lattice resonances and excitons in the donor-acceptor industry standard blend PDPPT5T:IEICO-4F.

Initial simulations were implemented to conclude which array dimensions, diameter and pitch, and thickness of the blend would result in the maximum short-circuit current when compared to a non-structured solar cell. The results showed a current enhancement of 15%. However, the complexity of this structure unables to probe the strong coupling between the collective resonances and the excitons states. Thus, simpler structures were simulate, where surface lattice resonances would spectrally overlap with the donor and/or acceptor of the organic blend. From these simulations, six metallic lattices were chosen to be fabricated with the following diameters (D) and pitches (P) - D70 P120, D70 P160, D100 P270, D120 P240, D130 P335 and D150 P420.

Anticipating experimental errors induced during the fabrication, different diameter arrays were prepared on glass substrates to study variations on the nanoparticles dimensions. After measuring the diameter of the nanoparticles with SEM and ImageJ Software, the overall diameters which best match the desired dimensions, are the ones projected with an offset of 10 nm, except for the two highest diameters where the best match was for an offset of 15 nm.

Spectrometry measurements of the gold nano disk lattice samples, coated with Polysterine, show different extinction spectras when compared to the simulated lattices. The experimental SLRs, emerging from lattices with diameters of 70nm, 100 nm and 120 nm do not overlap with either the donor or acceptor extinction spectras of PDPPT5T:IEICO-4F organic blend. The peaks, arising in the spectrometry results of the lattices coated with the organic blend, are emerge from the sum of the individual uncoupled states extinction spectras, and hence, do not emerge from coupling.

On the other hand, the SLRs of lattices with diameters of 130 and 150 nm overlap with both donor and acceptor extinction spectras of the PDPPT5T:IEICO-4F organic blend, resulting in the formation of visible peaks at 950 and 960 nm, respectively. Unlike the previous cases, these peaks result from the coupling of SLRs with PDPPT5T:IEICO-4F excitons (polaritons). The normalized extinction of the coupled system, with respect to the organic blend, shows the presence of a second peak for D=130 nm at approximately 650 nm, and a slight lump for D=150 nm, for the same wavelength. The latter could be indicating an upper polariton peak, however, the broad extinction of the PDPPT5T:IEICO-4F blend is possibly masking its appearance. Fourier measurements corroborate the results for the D=130 nm lattices, where two energies bands were also visible.

Two patterned substrates were prepared to deposit the nano disk arrays for the final solar cell devices and before coating the samples with the organic blend, ZnO and Ag layers, AFM measurements were done, to retrieve the diameters and height of the nanoparticles. Although the diameters embebbed in the solar cells

matched the ones studied before, the nano disk height was approximately 10 nm higher than the expected 30 nm - presumably due errors induced by the AFM the tip geometry.

Afterwards, the fabrication of two samples was completed: Sample A, where the metallic lattices were embedded in the ZnO layer and Sample B, where the metallic lattices were embedded in the organic blend layer. For the latter case, the devices were all short-circuited, demonstrating that it is unviable to deposit gold nanoparticles onto the ZnO layer. After measuring the J-V curves and retrieving the relevant solar cell parameters for sample A, it is clear that the Jsc, when compared to the reference, has experienced a slight decrease. This decrease is somewhat expected, considering the low Jsc percentage enhancement achieved with the simulations, the layer complexity of the final device structure and the increased reflectivity resulting from the incorporation of the metallic nanoparticles. The J-V measurements also demonstrated the possibility of incorporating metallic nanoparticle arrays in organic photovoltaics (thus changing its morphology) without degrading the cell's open-circuit voltage Voc. Similarly, the fill factor in sample A devices remained practically unchanged.

External quantum efficiency measurements were also performed on both samples, presenting similar results. In both cases, it was possible to affirm that the nanoparticle arrays have a strong influence on the EQE spectra shape, when compared to a non-nanostructured cell. The EQE spectra of these samples show again that the Jsc did not suffered a noticeable enhancement. Interestingly, it was possible to expand, even if by a small amount, the absorption edge of the blend towards infrared energies.

Despite the goal of achieving a short-circuit current enhancement by strong light matter coupling was not reached, this work demonstrated very promising results. From a material point of view, lattices of metallic nanoparticles introduced a reflectivity and losses to the system, hence other materials instead of metals, such as silicon, might be more advantageous. Additionally, different organic blend polymers could be investigated to exploit the maximum enhancement that polaritons states can provide. Lastly, for the specific application of transparent window photovoltaics, which is possible due to the transparency of the organic blend in the visible, the silver electrode could be replaced by a transparent material, such as ITO. From a geometrical point of view, several numerical optimizations can be done to reach the most favorable lattice dimensions and blend thickness, which were beyond the scope of this thesis.

BIBLIOGRAFIA

[1] O. A. Abdulrazzaq, V. Saini, S. Bourdo, E. Dervishi, and A. S. Biris, "Organic solar cells: A review of materials, limitations, and possibilities for improvement," *Part. Sci. Technol.*, vol. 31, no. 5, pp. 427–442, 2013, doi: 10.1080/02726351.2013.769470.

[2] S. Rafique, S. M. Abdullah, K. Sulaiman, and M. Iwamoto, "Fundamentals of bulk heterojunction organic solar cells: An overview of stability/degradation issues and strategies for improvement," *Renew. Sustain. Energy Rev.*, vol. 84, no. November 2017, pp. 43–53, 2018, doi: 10.1016/j.rser.2017.12.008.

[3] A. Khalil, Z. Ahmed, F. Touati, and M. Masmoudi, "Review on organic solar cells," *13th Int. Multi-Conference Syst. Signals Devices, SSD 2016*, pp. 342–353, 2016, doi: 10.1109/SSD.2016.7473760.

[4] J. M. Nunzi, "Organic photovoltaic materials and devices," *Comptes Rendus Phys.*, vol. 3, no. 4, pp. 523–542, 2002, doi: 10.1016/S1631-0705(02)01335-X.

[5] . V. K. A., "ORGANIC SOLAR CELLS: PRINCIPLES, MECHANISM AND RECENT DVELOPMENTS," *Int. J. Res. Eng. Technol.*, vol. 03, no. 09, pp. 338–341, Sep. 2014, doi: 10.15623/ijret.2014.0309053.

[6] M. T. Sajjad, A. Ruseckas, and I. D. W. Samuel, "Enhancing Exciton Diffusion Length Provides New Opportunities for Organic Photovoltaics," *Matter*, vol. 3, no. 2, pp. 341–354, Aug. 2020, doi: 10.1016/j.matt.2020.06.028.

[7] F. Enrichi and G. C. Righini, *Solar cells and light management: Materials, strategies and sustainability*. Elsevier, 2019.

[8] O. Sanchez-Sobrado *et al.*, "Lightwave trapping in thin film solar cells with improved photonic-structured front contacts," *J. Mater. Chem. C*, vol. 7, no. 21, pp. 6456–6464, 2019, doi: 10.1039/c8tc06092d.

[9] V. C. Nikolis *et al.*, "Strong light-matter coupling for reduced photon energy losses in organic photovoltaics," *Nat. Commun.*, vol. 10, no. 1, pp. 1–8, 2019, doi: 10.1038/s41467-019-11717-5.

[10] N. K. Elumalai and A. Uddin, "Open circuit voltage of organic solar cells: An in-depth review," *Energy Environ. Sci.*, vol. 9, no. 2, pp. 391–410, 2016, doi: 10.1039/c5ee02871j.

[11] M. Wang, M. Hertzog, and K. Börjesson, "Polariton-assisted excitation energy channeling in organic heterojunctions," *ChemRxiv*, pp. 1–25, 2020, doi: 10.26434/chemrxiv.12933011.v1.

[12] W. Wang, M. Ramezani, A. I. Väkeväinen, P. Törmä, J. G. Rivas, and T. W. Odom, "The rich photonic world of plasmonic nanoparticle arrays," *Mater. Today*, vol. 21, no. 3, pp. 303–314, 2018, doi: 10.1016/j.mattod.2017.09.002.

[13] P. Törmö and W. L. Barnes, "Strong coupling between surface plasmon polaritons and emitters: A review," *Reports Prog. Phys.*, vol. 78, no. 1, p. 13901, 2015, doi: 10.1088/0034-4885/78/1/013901.

[14] G. G. Rozenman, K. Akulov, A. Golombek, and T. Schwartz, "Long-Range Transport of Organic Exciton-Polaritons Revealed by Ultrafast Microscopy," *ACS Photonics*, vol. 5, no. 1, pp. 105–110, 2018, doi: 10.1021/acsphotonics.7b01332.

[15] G. W. Castellanos, P. Bai, and J. Gómez Rivas, "Lattice resonances in dielectric metasurfaces," *J. Appl. Phys.*, vol. 125, no. 21, 2019, doi: 10.1063/1.5094122.

[16] P. Bai, S. Ter Huurne, E. Van Heijst, S. Murai, and J. Gómez Rivas, "Evolutionary optimization of light-matter coupling in open plasmonic cavities," *J. Chem. Phys.*, vol. 154, no. 13, 2021, doi: 10.1063/5.0042056.

[17] A. M. Berghuis, V. Serpenti, M. Ramezani, S. Wang, J. Gómez Rivas, and J. Gómez Rivas, "Light-Matter Coupling Strength Controlled by the Orientation of Organic Crystals in Plasmonic Cavities," *J. Phys. Chem. C*, vol. 124, no. 22, pp. 12030–12038, 2020, doi: 10.1021/acs.jpcc.0c00692.

[18] J. Henson, J. Dimaria, and R. Paiella, "Influence of nanoparticle height on plasmonic resonance wavelength and electromagnetic field enhancement in two-dimensional arrays," *J. Appl. Phys.*, vol.

106, no. 9, 2009, doi: 10.1063/1.3255979.
[19] A. D. Utyushev, V. I. Zakomirnyi, and I. L. Rasskazov, “Collective lattice resonances: Plasmonics and beyond,” *Rev. Phys.*, vol. 6, no. September 2020, p. 100051, 2021, doi: 10.1016/j.revip.2021.100051.
[20] C. Dyer-Smith and J. Nelson, *Organic Solar Cells*. 2013.
[21] G. P. Smestad, *Optoelectronics of Solar Cells*, vol. 36, no. 6. SPIE, 2002.
[22] C. Acar and I. Dincer, “3.1 Hydrogen Production,” in *Comprehensive Energy Systems*, vol. 3–5, Elsevier, 2018, pp. 1–40.
[23] D. M. Coles *et al.*, “Polariton-mediated energy transfer between organic dyes in a strongly coupled optical microcavity,” *Nat. Mater.*, vol. 13, no. 7, pp. 712–719, Jul. 2014, doi: 10.1038/nmat3950.
[24] M. Tian, X. Li, Z. Li, and X. Zhong, “Analysis of the Forward and Reverse Strongly Coupled States on the Nonradiative Energy Transfer Effect,” *J. Phys. Chem. Lett.*, vol. 12, no. 20, pp. 4944–4950, May 2021, doi: 10.1021/acs.jpclett.1c01088.
[25] K. Nagarajan *et al.*, “Conductivity and Photoconductivity of a p-Type Organic Semiconductor under Ultrastrong Coupling,” *ACS Nano*, vol. 14, no. 8, pp. 10219–10225, 2020, doi: 10.1021/acsnano.0c03496.
[26] E. Orgiu *et al.*, “Conductivity in organic semiconductors hybridized with the vacuum field,” *Nat. Mater.*, vol. 14, no. 11, pp. 1123–1129, 2015, doi: 10.1038/nmat4392.
[27] M. Litinskaya, “Polaritons,” *Encycl. Condens. Matter Phys.*, pp. 334–341, 2005, doi: 10.1016/B0-12-369401-9/00663-X.
[28] X. Zhong *et al.*, “Energy Transfer between Spatially Separated Entangled Molecules,” *Angew. Chemie - Int. Ed.*, vol. 56, no. 31, pp. 9034–9038, 2017, doi: 10.1002/anie.201703539.
[29] X. Zhong *et al.*, “Non-radiative energy transfer mediated by hybrid light-matter states,” *Angew. Chemie - Int. Ed.*, vol. 55, no. 21, pp. 6202–6206, 2016, doi: 10.1002/anie.201600428.
[30] S. Gambino *et al.*, “Exploring Light-Matter Interaction Phenomena under Ultrastrong Coupling Regime,” *ACS Photonics*, vol. 1, no. 10, pp. 1042–1048, 2014, doi: 10.1021/ph500266d.
[31] V. Agranovich, *Excitations in Organic Solids*, vol. 3rd. Oxford University Press, 2008.
[32] N. Yao *et al.*, “Efficient Charge Transport Enables High Efficiency in Dilute Donor Organic Solar Cells,” *J. Phys. Chem. Lett.*, vol. 12, no. 20, pp. 5039–5044, 2021, doi: 10.1021/acs.jpclett.1c01219.
[33] C. A. DelPo, S.-U.-Z. Khan, K. H. Park, B. Kudisch, B. P. Rand, and G. D. Scholes, “Polariton Decay in Donor–Acceptor Cavity Systems,” *J. Phys. Chem. Lett.*, pp. 9774–9782, 2021, doi: 10.1021/acs.jpclett.1c02644.
[34] V. Giannini, A. I. Fernández-Domínguez, S. C. Heck, and S. A. Maier, “Plasmonic nanoantennas: Fundamentals and their use in controlling the radiative properties of nanoemitters,” *Chem. Rev.*, vol. 111, no. 6, pp. 3888–3912, 2011, doi: 10.1021/cr1002672.
[35] P. Bharadwaj, B. Deutsch, and L. Novotny, “Optical Antennas,” *Adv. Opt. Photonics*, vol. 1, no. 3, p. 438, 2009, doi: 10.1364/aop.1.000438.
[36] P. Biagioni, J. S. Huang, and B. Hecht, “Nanoantennas for visible and infrared radiation,” *Reports Prog. Phys.*, vol. 75, no. 2, 2012, doi: 10.1088/0034-4885/75/2/024402.
[37] L. Feng, M. Niu, Z. Wen, and X. Hao, “Recent advances of plasmonic organic solar cells: Photophysical investigations,” *Polymers (Basel).*, vol. 10, no. 2, pp. 1–33, 2018, doi: 10.3390/polym10020123.
[38] H. Gao *et al.*, “Rayleigh anomaly-surface plasmon polariton resonances in palladium and gold subwavelength hole arrays,” *Opt. Express*, vol. 17, no. 4, p. 2334, 2009, doi: 10.1364/oe.17.002334.
[39] W. A. Murray and W. L. Barnes, “Plasmonic materials,” *Adv. Mater.*, vol. 19, no. 22, pp. 3771–3782, 2007, doi: 10.1002/adma.200700678.
[40] K. L. Kelly, E. Coronado, L. L. Zhao, and G. C. Schatz, “The Optical Properties of Metal Nanoparticles: The Influence of Size, Shape, and Dielectric Environment,” *J. Phys. Chem. B*, vol. 107, no. 3, pp. 668–677, Jan. 2003, doi: 10.1021/jp026731y.
[41] J. You, Y. Takahashi, K. Leonard, H. Yonemura, and S. Yamada, “Influence of space arrangement of silver nanoparticles in organic photoelectric conversion devices,” *J. Photochem. Photobiol. A Chem.*, vol. 332, pp. 586–594, 2017, doi: 10.1016/j.jphotochem.2016.09.023.
[42] S. Collin, “Nanostructure arrays in free-space: Optical properties and applications,” *Reports Prog. Phys.*, vol. 77, no. 12, 2014, doi: 10.1088/0034-4885/77/12/126402.
[43] L. Hüttenhofer *et al.*, “Metasurface Photoelectrodes for Enhanced Solar Fuel Generation,” *Adv. Energy Mater.*, p. 2102877, Oct. 2021, doi: 10.1002/aenm.202102877.
[44] R. K. Yadav *et al.*, “Strongly Coupled Exciton-Surface Lattice Resonances Engineer Long-Range

Energy Propagation," *Nano Lett.*, vol. 20, no. 7, pp. 5043–5049, 2020, doi: 10.1021/acs.nanolett.0c01236.
[45] J. Robinson and Y. Rahmat-Samii, "Particle swarm optimization in electromagnetics," *IEEE Trans. Antennas Propag.*, vol. 52, no. 2, pp. 397–407, 2004, doi: 10.1109/TAP.2004.823969.
[46] T. P. A. van der Pol, J. Li, B. T. van Gorkom, F. J. M. Colberts, M. M. Wienk, and R. A. J. Janssen, "Analysis of the performance of narrow-bandgap organic solar cells based on a diketopyrrolopyrrole polymer and a nonfullerene acceptor," *J. Phys. Chem. C*, vol. 125, no. 10, pp. 5505–5517, 2021, doi: 10.1021/acs.jpcc.0c11377.
[47] X. Zhang, J. Qiu, X. Li, J. Zhao, and L. Liu, "Complex refractive indices measurements of polymers in visible and near-infrared bands," *Appl. Opt.*, vol. 59, no. 8, p. 2337, 2020, doi: 10.1364/ao.383831.

A. EBL parameters used for each array dimensions.

Table 6 - EBL parameters used for each array dimensions.

Array No.	Array Dimensions		Current (nA)	Beam Size (nm)	Beam Step Size (nm)	Dose ($\mu m/cm^2$)
	Diameter (nm)	Pitch (nm)				
1	70	120	2	18	4	1100
2	70	140	2	18	4	1100
3	70	160	2	18	4	1100
4	70	180	2	18	4	1100
5	100	270	2	18	4	1100
6	100	290	2	18	4	1100
7	120	240	2	18	4	1100
8	120	260	2	18	4	1100
9	130	335	2	18	4	1100
10	130	355	2	18	4	1100
11	150	420	2	18	4	1100
12	150	450	2	18	4	1100
13	120	240	30	31	4	1200
14	120	260	30	31	4	1200
15	130	335	30	31	4	1200
16	130	355	30	31	4	1200
17	150	420	30	31	4	1200
18	150	450	30	31	4	1200

B. Organic blend n and k values.

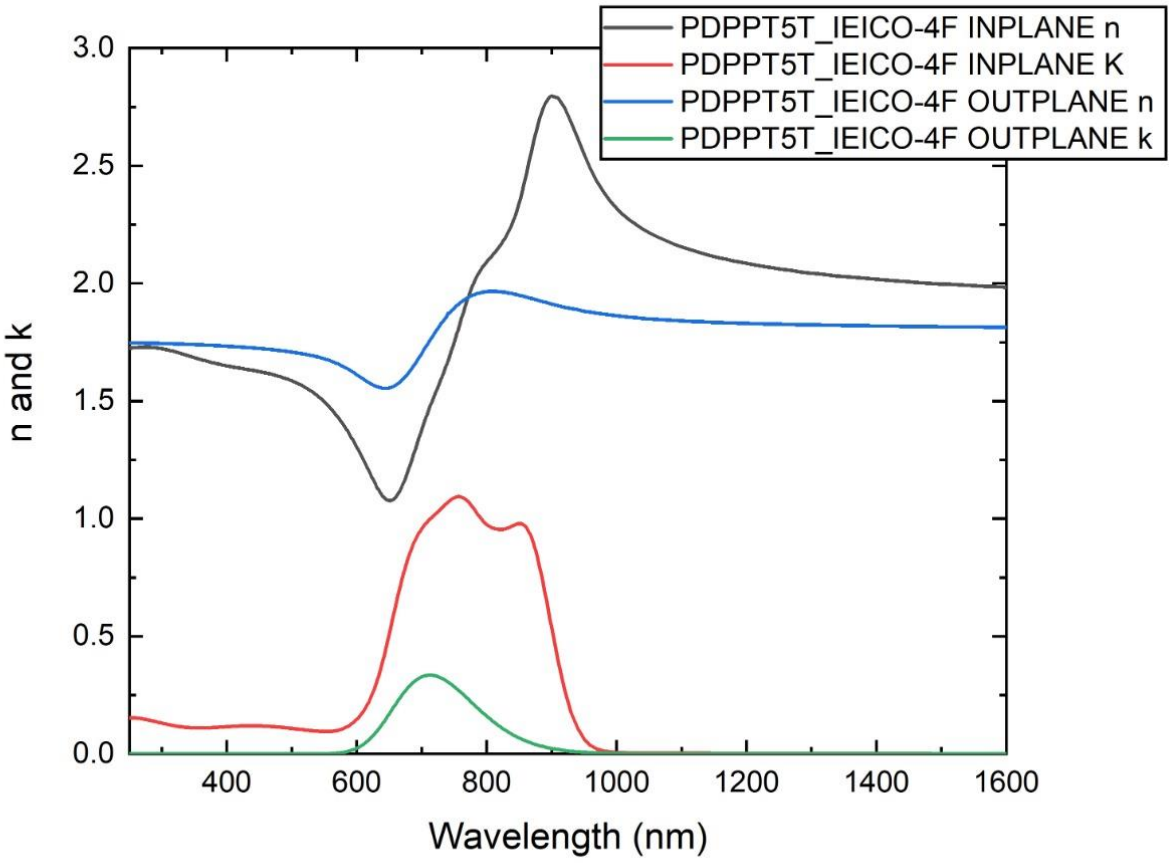

Figure 5.1 -PDPPT5T:IEICO-4F organic blend n (refractive index) and k (extinction coefficient) values for in-plane (IP) and out-of-plane (OOP) dispersion.

C. Extinction Formula.

$$Extinction = 1 - \frac{T_{Sample} - T_{Dark}}{T_{Reference} - T_{Dark}}$$

Where T is Transmission.

D. Fourier Microscopy Setup.

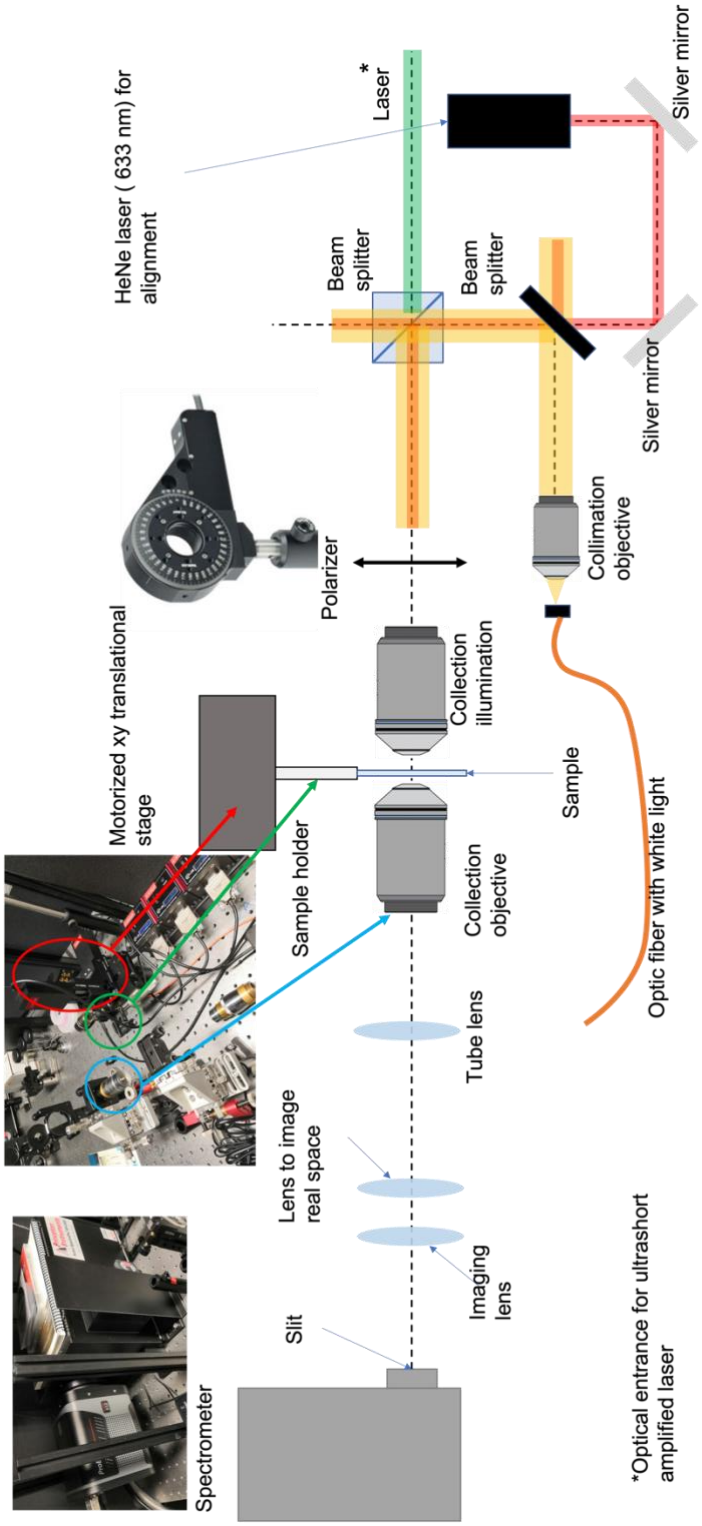

2021

TOMÁS ALEXANDRE DE SOUSA

STRONG LIGHT-MATTER COUPLING FOR IMPROVED ORGANIC PHOTOVOLTAICS

NOVA SCHOOL OF SCIENCE & TECHNOLOGY